AN ABSTRACT OF THE THESIS OF

JON ROBERT LOSEE (Name) for the DOCTOR OF PHILOSOPHY (Degree)

in PHYSICS (Major) presented on July 30, 1971 (Date)

Title: EXPERIMENTAL ELECTRON ENERGY DISTRIBUTIONS FOR TOWNSEND DISCHARGES IN ARGON GAS

Abstract approved: Redacted for privacy
David S. Burch

In this work the electron energy distribution functions and the anisotropic drift term of the velocity distribution functions in non-selfsustaining (Townsend) discharges in argon were determined by direct measurement for a range of E/N (electric field strength by gas atom concentration) from 70 to 407 Townsends (Td). (One Td equals 10^{-17} volts-cm^2). Motivation is supplied by the theoretical prediction by Heylen and Lewis (9) of unusual electron energy distributions in Townsend discharges in the noble gases, and by the subsequent work by Roberts and Burch (20) supporting this prediction in helium. Some structure in the form of the distribution functions is observed, but the prediction of Heylen and Lewis (9) for argon is not fully supported.

The experimental method employed is to energy-analyse electrons effusing from apertures in the anode of a discharge cell with a

spherical retarding electric field. The discharge cell has plane parallel electrodes, a guard ring for field uniformity, and a specially built perforated anode. To determine the effect on the measurement of collecting the effusing electrons with a non-ideal collector, the collection efficiency of a platinum blacked stainless steel collector was investigated. Also, an attempt was made to insure the sphericity of the retarding field; however, the perturbations due to the non-spherical part of the field were also analyzed.

The experimental energy distributions were used along with cross section data from the literature to compute the electron mobilities, diffusion constants, mean energies, and Townsends first ionization coefficients. Combination of the data with results from kinetic theory permitted evaluation of the anisotropic part of the velocity distribution function.

Experimental Electron Energy Distributions for Townsend Discharges in Argon Gas

by

Jon Robert Losee

A THESIS

submitted to

Oregon State University

in partial fulfillment of
the requirements for the
degree of

Doctor of Philosophy

June 1972

APPROVED:

Redacted for privacy

Professor of Physics

in charge of major

Redacted for privacy

Chairman of Department of Physics

Redacted for privacy

Dean of Graduate School

Date thesis is presented July 30, 1971

Typed by Clover Redfern for Jon Robert Losee

ACKNOWLEDGMENTS

I sincerely appreciate the guidance and encouragement supplied by my major professor, Dr. David S. Burch.

I also would like to thank Dr. James C. Looney of the Oregon State University Electrical Engineering Dept. for his cooperation in the photoetching of gold foils.

TABLE OF CONTENTS

	Page
INTRODUCTION	1
THEORY OF OPERATION	6
EQUIPMENT AND DETAILS	12
The Vacuum System	12
The Gas Handling System	14
The Guard Sphere	15
The Electron Gun	16
The Collector	16
The Discharge Cell	20
The Anode	22
Electrical Circuits	27
DATA AND ANALYSIS	30
RESULTS	43
CONCLUSIONS	61
BIBLIOGRAPHY	63
APPENDICES	66
Appendix A	66
Appendix B	67

LIST OF FIGURES

Figure		Page
1.	Electron energy distribution functions for helium at E/N - 140 Td.	4
2.	Electron energy distribution function for argon at 282 Td calculated by Heylan and Lewis (9).	5
3.	Simplified schematic of discharge cell and energy analyzer.	8
4.	Block diagram of gas handling system and vacuum system.	13
5.	Electron gun.	17
6.	Electron collection efficiencies.	19
7.	Block diagram of electrical circuits.	28
8.	Typical chart recorder signal.	31
9.	Typical collector current vs retarding voltage curve at E/N = 350 Td.	33
10.	Sample curve for the determination of the no-gas distortion function for 8 volt electrons.	36
11.	Normalized energy distribution functions using the GR diffusion cross section.	44
12.	Normalized energy distribution functions at E/N = 282 Td for two choices of the diffusion cross section.	50
13.	Normalized distribution functions $F_0(\epsilon)$ and $F_1(\epsilon)$ at E/N = 407 Td.	52
14.	Townsend's first ionization coefficient vs E/N.	56
15.	Semi-log graph of discharge current vs pressure at E/N = 210 Td.	58

LIST OF TABLES

Table		Page
1.	Table of normalized electron distribution functions in argon using the GR diffusion cross section.	45
2.	Table of normalized electron distribution functions in argon using the MB diffusion cross section.	47
3.	Table of transport quantities.	55

EXPERIMENTAL ELECTRON ENERGY DISTRIBUTIONS FOR TOWNSEND DISCHARGES IN ARGON GAS

INTRODUCTION

When electrons pass through a gas under the influence of a uniform electric field, they undergo collisions with the gas and, under certain conditions, an equilibrium state results from the forcing effect of the field and the retarding influence of collisions. This state depends on the type of gas, the gas concentration N, and the applied electric field E. A description of the physical situation is afforded by definition of a function $f(\underline{r}, \underline{v}, t)$ such that $f(\underline{r}, \underline{v}, t)d\underline{r}d\underline{v}$ is the ensemble average number of electrons at time t which lie in a volume $d\underline{r}$ at $\underline{r}$ and whose velocity lies within the volume $d\underline{v}$ at $\underline{v}$, where $\underline{r}$ is a position vector in configuration space and $\underline{v}$ is a position vector in velocity space. It is then necessary to find an equation solved by $f(\underline{r}, \underline{v}, t)$ and, finally, to solve the equation. Since electrons can change either their position or velocity only by moving, being accelerated, or by collisions, there results the following equation: $\underline{v} \cdot \nabla f + \underline{E}e/m \cdot \nabla_v f + \partial f/\partial t = Df$, where ∇f is the gradient of f in configuration space, $\nabla_v f$ is the gradient in velocity space, e is the charge of an electron, m is the mass of an electron, and Df is the net change per unit time of f due to collisions. This equation is known as the Boltzmann Equation.

As mentioned before, the state which f describes depends on the gas, the electric field, and the gas pressure. The way in which f depends on electric field and gas pressure was first inferred by Townsend. Townsend investigated non-selfsustaining gas discharges between plane parallel electrodes and found, for a range of discharge conditions, that the discharge current had the form: $I = I_0 \exp(\alpha d)$, where I_0 is the initial electron current from the cathode, d is the distance between the electrodes, and α is the number of new ion pairs created per electron per cm of path in the direction of the electric field by one primary electron. The parameter α is called Townsend's first ionization coefficient. Townsend found that, at constant temperature, α/p is a function of E/p only. Other investigations showed that, under similar conditions, parameters such as $p\mu$ and pD were functions of E/p only. Here μ is the electron mobility, defined as drift velocity per unit field strength, and D is the diffusion constant. That these transport quantities are functions of E/p only in a certain range implies that $f(\underline{r}, \underline{v}, t)$ is also a function of E/p only. The non-selfsustaining gas discharges characterized by E/p are now called Townsend discharges. In order to take account of gas temperature the parameter E/p is, nowadays, replaced by E/N, where N is the number of molecules per cc. This work will use the parameter E/N to describe the discharges investigated.

Efforts in the past to find $f(\underline{r}, \underline{v}, t)$ have generally used indirect methods. Some examples are: probe studies of plasmas, measuring transport phenomena such as diffusion, electrical conductivity, and drift velocity and then using these to infer f, and theoretical solutions to the Boltzmann equation under certain assumptions.

Heylen and Lewis (9) completed a work in 1962 in which distributions were derived for Townsend discharges in some of the noble gases. Their work used both the Boltzmann equation and experimental cross section data for elastic and inelastic electron-molecule collisions. Their conclusions showed some dramatic structure in the form of the energy distribution functions. This predicted structure prompted an investigation in 1964 by Roberts and Burch (20) to determine whether the structure could be observed experimentally. Their work showed some agreement with the structure or "break" in the distribution function as predicted by Heylen and Lewis (9) in helium. See Figure 1.

Since the structure predicted by Heylen and Lewis (9) is much more pronounced for argon than for helium, Figure 2, it was believed that an investigation of argon might be fruitful and interesting, and this job was undertaken here. The retarding field method of measuring electron distribution functions as used by Roberts and Burch (20) is used here with some modifications. The main modifications are to the discharge cell and to the analysis of the data as will become evident in later chapters.

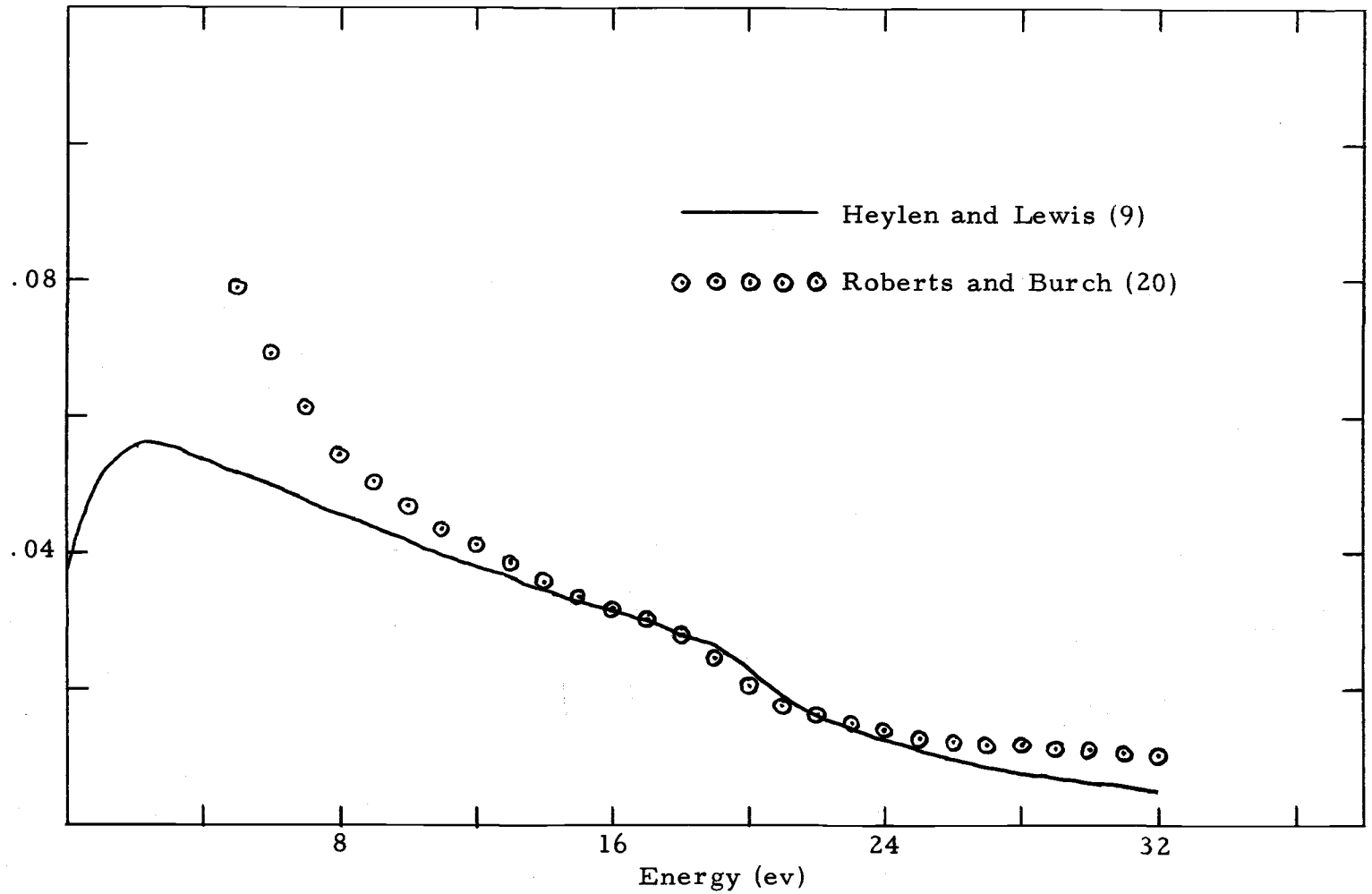

Figure 1. Electron energy distribution functions for helium at E/N = 140 Td.

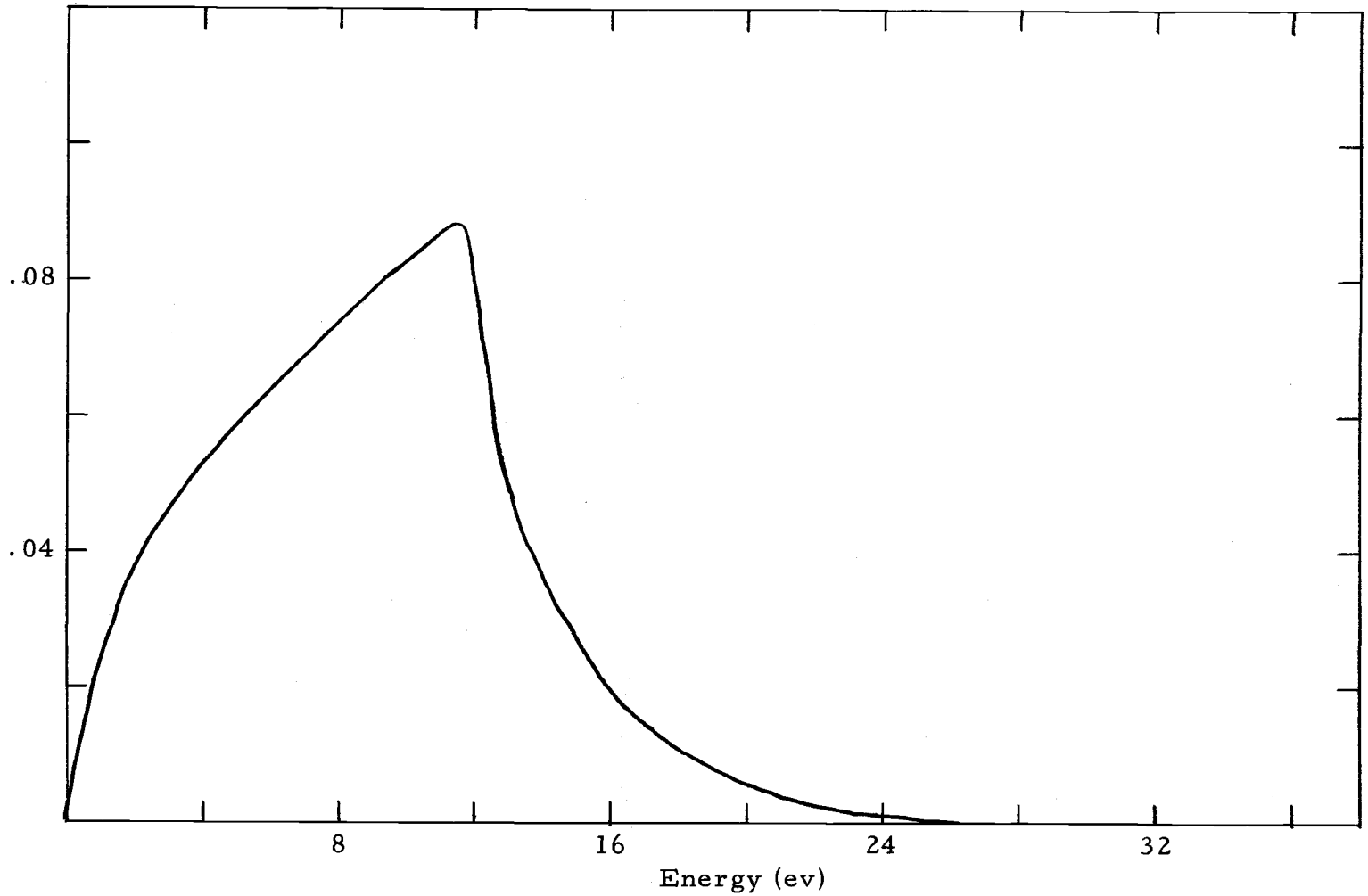

Figure 2. Electron energy distribution function for argon at 282 Td calculated by Heylan and Lewis (9).

THEORY OF OPERATION

In this chapter particle flow through an aperture is discussed, along with the connection between electron flux and the energy distribution function. This connection forms a basis for the experimental approach.

When a small aperture is introduced into the anode of a gas discharge, electrons and gas atoms escape in either of two limiting ways, hydrodynamic flow and effusive flow. In hydrodynamic flow a pressure gradient is produced in the gas behind the aperture due to the large loss of atoms in the vicinity of the aperture. This pressure gradient, in turn, drives the gas toward and through the aperture. An analysis of this case would not prove fruitful to this work because the energy distribution of escaping electrons is distorted by the pressure gradient, and is, therefore, not characteristic of a Townsend discharge. In the effusive flow case, however, few atoms escape because only those atoms whose velocities are directed toward the aperture, and which are sufficiently near that they do not suffer a collision, are able to escape. Since few atoms escape, the pressure at the back of the aperture is inappreciably altered. Thus, once the electrons have reached equilibrium with the gas and electric field, their energy distribution should not be spacially dependent, except for lateral diffusion, and the escaping electrons are representative of a

Townsend discharge. By energy analysis of these effusing electrons, their energy distribution in the discharge can be deduced. The energy analysis is accomplished by a retarding electric field between the discharge cell (anode) and a segment of a collecting sphere, see Figure 3. To make the connection between the energy analysis of the effusing electrons and the energy distribution of electrons in the discharge, the flux of effusing electrons must be calculated.

In an equilibrium situation with no spacial dependence $f(\underline{r}, \underline{v}, t)$ becomes simply $f(\underline{v})$; then P, the flux of particles crossing a surface of unit area per unit time, is

$$P = \int f(\underline{v}) v \cos \theta d\underline{v},$$

where θ is the angle between the velocity direction and the normal to the surface. In spherical coordinates,

$$P = \int_0^{\infty} \int_0^{\theta_m} \int_0^{2\pi} f(\underline{v}) v^3 \cos \theta \sin \theta d\theta d\phi dv,$$

where θ_m is the maximum angle subtended by the collector. For nearly isotropic velocity distributions, $f(\underline{v})$ can be expanded in Lengendre polynomials as follows:

$$f(\underline{v}) = f_0(v) + f_1(v) \cos \theta,$$

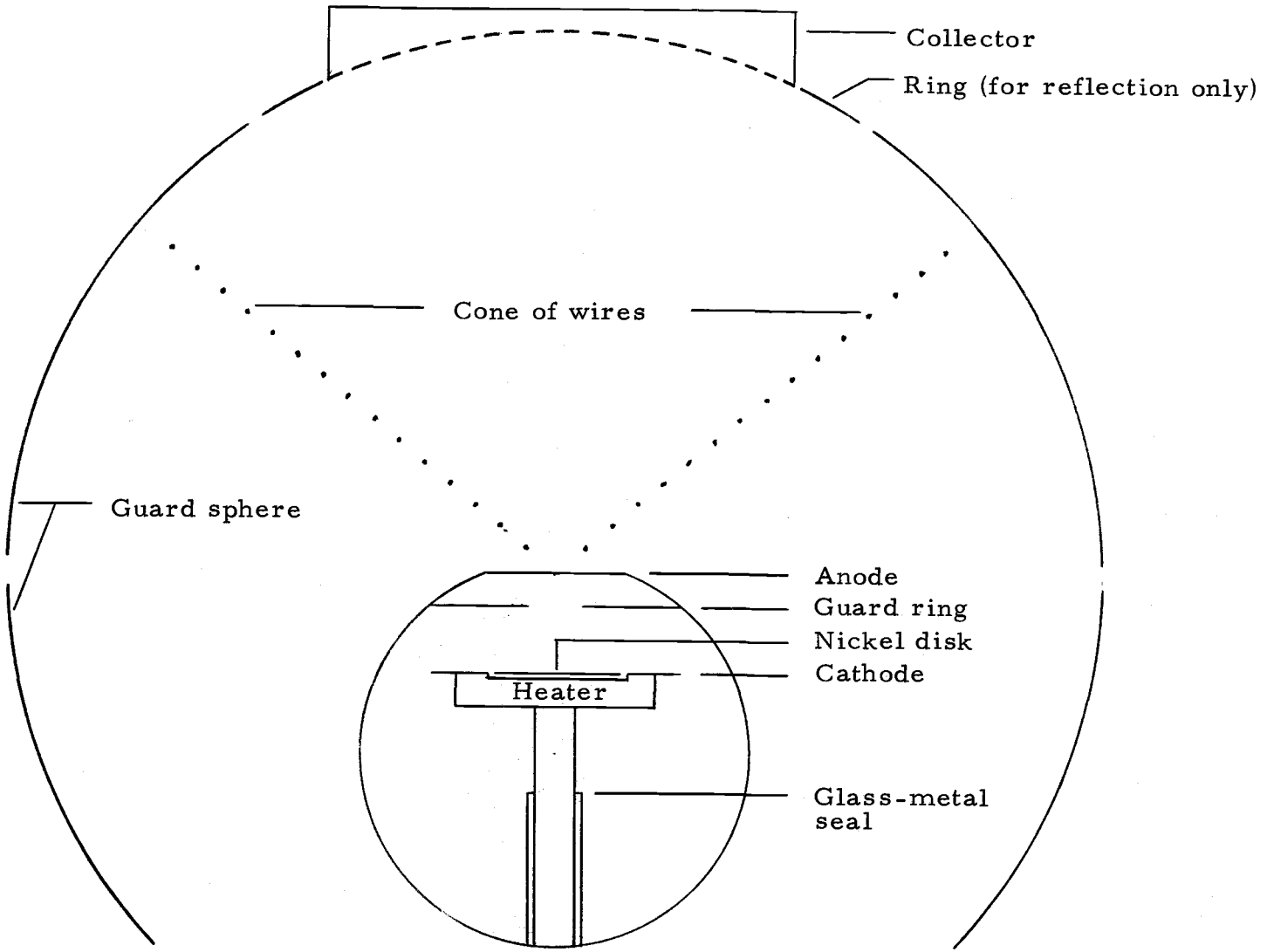

Figure 3. Simplified schematic of discharge cell and energy analyzer.

where $f_0(v)$ is the isotropic term, $f_1(v)$ is the term responsible for drift, and terms in $P_2(\cos\theta)$ and higher are assumed small and are dropped. Thus, assuming a nearly isotropic velocity distribution and cylindrical symmetry, the angular integrations can be performed and P becomes:

$$P = \pi \sin^2\theta_m \int_0^\infty [f_0(v) + \frac{2(1-\cos^3\theta_m)}{3\sin^2\theta_m} f_1(v)]v^3 dv .$$

For this experiment, $\theta_m = .473$ radians, and evaluating the above term gives:

$$P = \pi \sin^2\theta_m \int_0^\infty [f_0(v) + .945 f_1(v)]v^3 dv.$$

Substituting $\frac{1}{2}mv^2 = \epsilon$ and lumping constants, we have:

$$P = k \sin^2\theta_m \int_0^\infty [f_0(\epsilon) + .945 f_1(\epsilon)]\epsilon d\epsilon .$$

In the experiment, the flux to the collector, P_c, is that which can overcome the retarding potential V applied between the cell and the collector:

$$P_c = k \sin^2\theta_m \int_V^\infty [f_0(\epsilon) + .945 f_1(\epsilon)]\epsilon d\epsilon .$$

Then the current I received at the collector is, in arbitrary units:

$$I(V) = \int_V^\infty [f_0(\epsilon) + .945 f_1(\epsilon)]\epsilon \, d\epsilon .$$

The fact that $f_1(\epsilon)$ appears in this expression for I means that the experiment alone does not discriminate against its effects. $f_1(\epsilon)$ must be either eliminated or otherwise accounted for because, since energy is a scalar quantity, the electron energy distribution function depends on $f_0(\epsilon)$ only, terms of higher order giving zero when integrated over all angles in velocity space. In this work, $f_1(\epsilon)$ is accounted for by using the following relationship derived from kinetic theory. By using the above approximation for $f(\underline{v})$ in the Boltzmann transport equation, two coupled equations for f_0 and f_1 are obtained (1). After some manipulations and approximations, one of these equations gives f_1 in terms of f_0 as follows:

$$f_1(\epsilon) = -(E/p)[1/(P_d(\epsilon) + Q_{in}(\epsilon))](d/d\epsilon) f_0(\epsilon),$$

where $P_d(\epsilon)$ is the diffusion cross section in cm^{-1} and $Q_{in}(\epsilon)$ is the total inelastic cross section in cm^{-1}. The expression for the collector current in terms of $f_0(\epsilon)$ is:

$$I(V) = \int_V^\infty [f_0(\epsilon) - .945(E/p)[1/(P_d(\epsilon) + Q_{in}(\epsilon))](d/d\epsilon) f_0(\epsilon)]\epsilon \, d\epsilon .$$

It is useful at this point to define the energy distribution function and to obtain a first approximation for it. Since $f_0(v)v^2dv$ is the number of particles in dv with speed v, then $f_0(\epsilon)\epsilon^{1/2}d\epsilon$ is the number of particles in $d\epsilon$ with energy at ϵ. Define $F_0(\epsilon)d\epsilon = f_0(\epsilon)\epsilon^{1/2}d\epsilon$; then $F_0(\epsilon)$ is the energy distribution function. For continuity an anisotropic part $F_1(\epsilon)$ is defined to be $f_1(\epsilon)\epsilon^{1/2}$. To obtain a first approximation to $F_0(\epsilon)$, the second term in the integrand in the expression for the collector current is dropped; then I is given by:

$$I(V) = \int_V^\infty F_0(\epsilon)\epsilon^{1/2}d\epsilon.$$

Therefore, differentiating the collector current with respect to the retarding voltage and dividing by $V^{1/2}$ gives the desired approximation.

An assumption made in deriving the above expressions for the collector current is that all electrons with energies greater than V will be received at the collector. In the experiment it is found that this assumption is invalidated by the defocusing of the electron beam due to the retarding field and by electron reflection at the collector. The necessary modification of the above theory to include these effects will be presented in the section on data analysis.

EQUIPMENT AND DETAILS

Discussed in this chapter will be the actual experimental apparatus, construction details, and, where appropriate, the conditions and tests that must be satisfied by each particular component. The discussion is broken up into the following sections: vacuum system, gas handling system, the guard sphere, the electron gun, the collector, the discharge cell, the anode, and the electrical circuits.

The Vacuum System

The vacuum and gas handling systems will be discussed with reference to the plumbing schematic, Figure 4. The system was roughed through a liquid nitrogen trap by an Edwards 15 cfm mechanical pump connected in parallel with a Cenco Hyvac 7. With the trap filled, the forepressure achieved was about 1 micron of Hg, as measured with a NCR thermocouple gauge, and was not affected by gas in the cell or operation of the diffusion pump. On the other side of the trap was a CVC 6-inch oil diffusion pump charged with Dow Corning 704 silicone oil and above it was a CVC 6 inch baffle refrigerated with freon-12. Mounted directly over the baffle was the vacuum can, which was a nickel-plated steel cylinder 10 inches high and 12 inches in diameter. The base pressure in the can depended heavily on the adjustment of the refrigeration system; however, with optimum

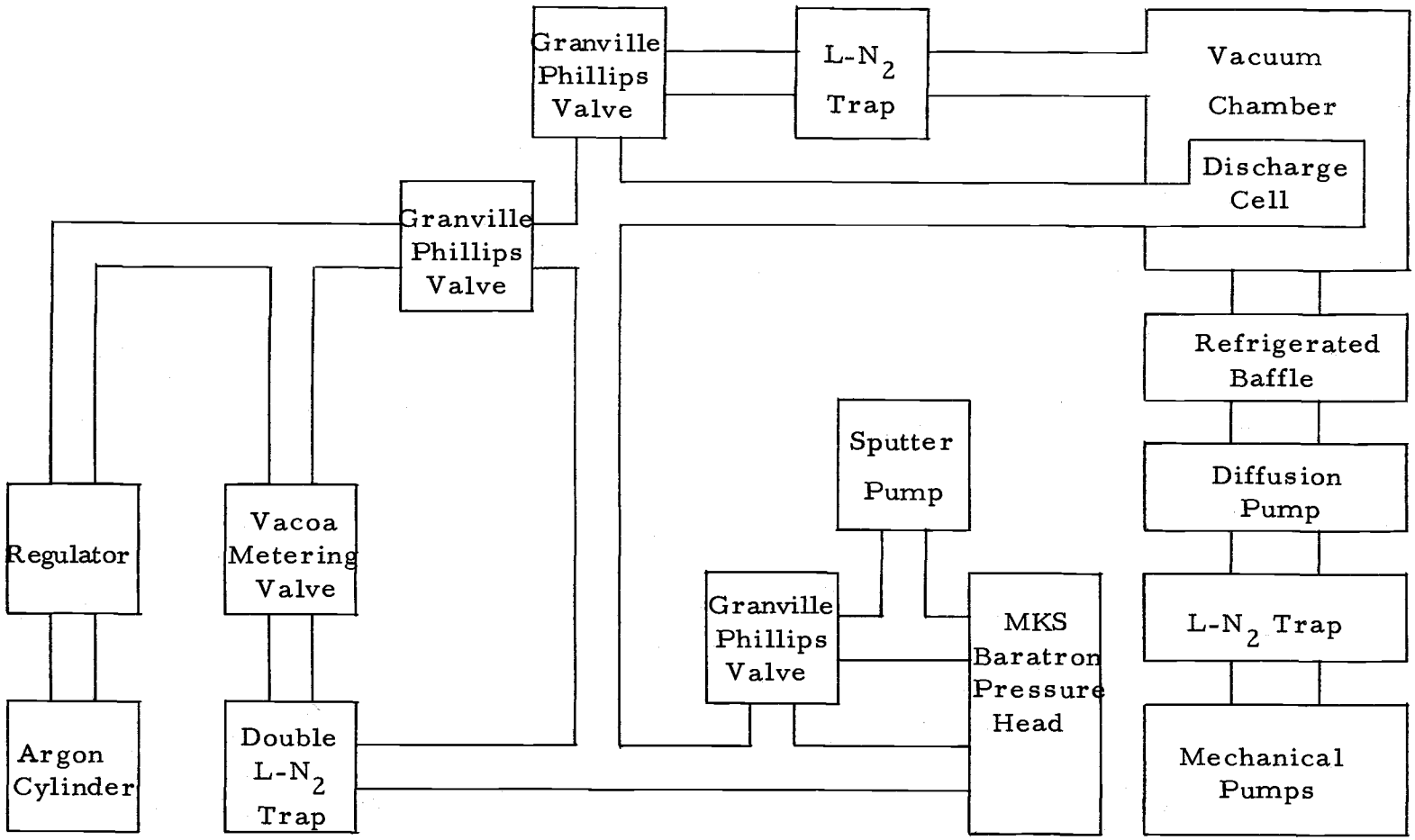

Figure 4. Block diagram of gas handling system and vacuum system.

throttle valve adjustment, pressures of 8×10^{-7} torr with no gas in the cell and 5×10^{-6} torr with one torr of gas in the cell were obtained. The pressures were measured with a Veeco RG-21A ionization gauge whose tube was mounted directly on the side of the can.

The Gas Handling System

The source of argon was a 50 liter lecture bottle of Matheson research grade argon with a manufacturers' listed impurity of less than 3 ppm nitrogen. The bottle was fitted with a model 3500 stainless steel regulator whose outlet pressure was run at about 3 lbs/sq inch, gauge. The gas flow and, thus, the cell pressure, were then controlled by a Vacoa model MV-25-XL stainless steel metering valve; this valve enabled the cell pressure to be established to within ±1 micron of Hg. The gas at the outlet side of the Vacoa valve was passed through a double liquid nitrogen trap (which was the only purification measure taken) before it entered the cell. A by-pass around the double trap and Vacoa valve aided in pumping the system back to the argon bottle. All other valves in the gas handling system were Granville-Phillips ultrahigh vacuum valves. The cell pressures were measured with a M.K.S. Baratron pressure meter equipped with a 10 torr head. The reference pressure for the head was fixed by use of a 1 liter/sec sputter pump, and usually ran at about 10^{-6} torr. The entire gas handling system, including the cell, was pumped

through a liquid nitrogen trap connected to the vacuum can to at least 10^{-6} torr before any argon was introduced.

The Guard Sphere

A stainless steel sphere of ID 4.38 inches surrounded the cell to act as an electrostatic shield and, more importantly, to help establish a spherically symmetric retarding electric field. The sphere was sectioned into an upper and lower hemisphere for convenience of assembly. A hole was cut in the top of the upper hemisphere for installation of the collector, which will be described later. The sphere was then gold blacked on the inside to help prevent any reflected electrons from reaching the collector. Inside the top hemisphere a cone of wire circles spaced 1/2 cm apart was used to help establish the spherical symmetry of the field in the analyzing region. Each loop was held at the potential correct for its particular radius by a chain of resistors which were coated with Torr-Seal resin and connected from loop to loop inside the vacuum can. To calculate the potential of each loop, the total potential was taken as if between two concentric spheres of 1/4 cm and 11 cm radius respectively.

A different sphere was used for the electron reflection work; this sphere was similar to the one described above but, in addition, was further segmented by cutting a ring adjacent to the collector. The ring was electrically isolated so that current to it could be

measured. The cell was replaced by an electron gun and no guard cone was employed.

The Electron Gun

This element is shown schematically in Figure 5. The cathode assembly from a CRT tube was spot welded to a 1/2 inch diameter collimating tube 3.5 cm long. The tube contained three 1.5 mm apertures, one at each end and one 1 cm from the top. These apertures confined the electron beam to ensure that it would strike the collector segment only. Geometric rather than electrostatic collimation was used because the energy of the electrons was changed over a wide range, and this type of collimation is independent of energy.

The Collector

A segment of the guard sphere, 4 inches across, centered on the axis of the discharge cell, and subtending a plane angle from this axis of .473 radians was modified and used to collect the effusing electrons. It was electrically isolated from the rest of the sphere by three glass rods, each about 2 cm long. To help prevent electron reflection, this segment was made from a stainless steel cup 3/4 inch deep and 4 inches in diameter, and covered with a spherically shaped 30 mesh stainless steel screen. Both the cup and screen were platinum blacked. The platinum black surface is used because of its

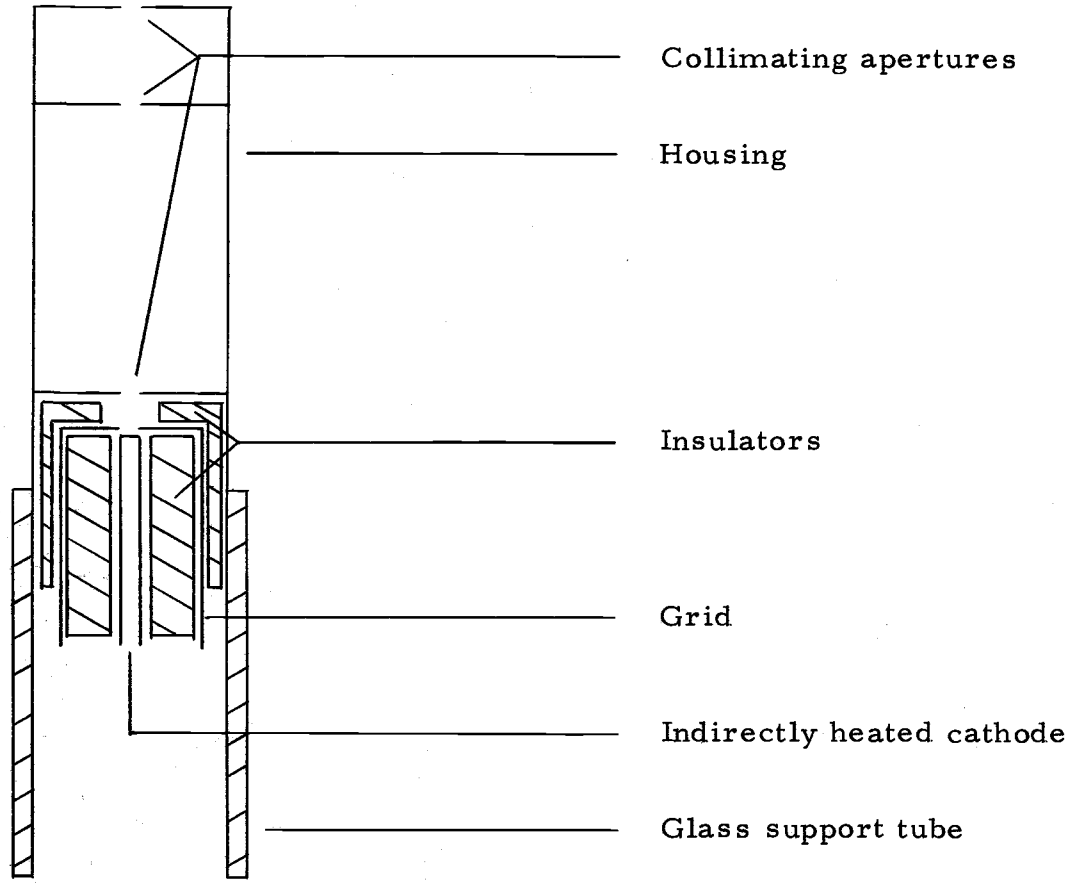

Figure 5. Electron gun.

exceptional ability to prevent electron reflection. The black is formed by electroplating from a solution of 3 grams platinic chloride and .025 grams lead acetate to 100 cc of water. The plating is accomplished by passing the current from a 4 volt source for 5 to 10 minutes, reversing the direction of the current every 30 seconds (14). Because the solution is very reactive, the process can be used only on relatively inert metals such as stainless steel, platinum, gold, etc. The reflection characteristics of this collector shown in Figure 6 were obtained by using the collimated electron gun mounted at the center of the guard sphere. The currents to the collector, the ring, and the guard sphere were measured as a function of electron energy by Keithly model 600A electrometers. Then, the fraction of electrons collected by the collector is $I_c/(I_c+I_r+I_g)$, where I_c is the collector current, I_r is the ring current, and I_g is the guard sphere current. To insure that I_r and, thus, I_g resulted primarily from reflected electrons, the data were retaken with the electron gun 1-1/2 inches nearer the collector. If primary electrons had been collected on the ring with the gun at the center of the guard sphere, then the flux due to these should decrease with the gun nearer the collector and, consequently, the ratio of ring current to collector current should decrease. The data showed that, in fact, the ratio increased as the gun was moved nearer the collector. Therefore, the fraction of I_r which is due to primary electrons must be small. Since the ring and

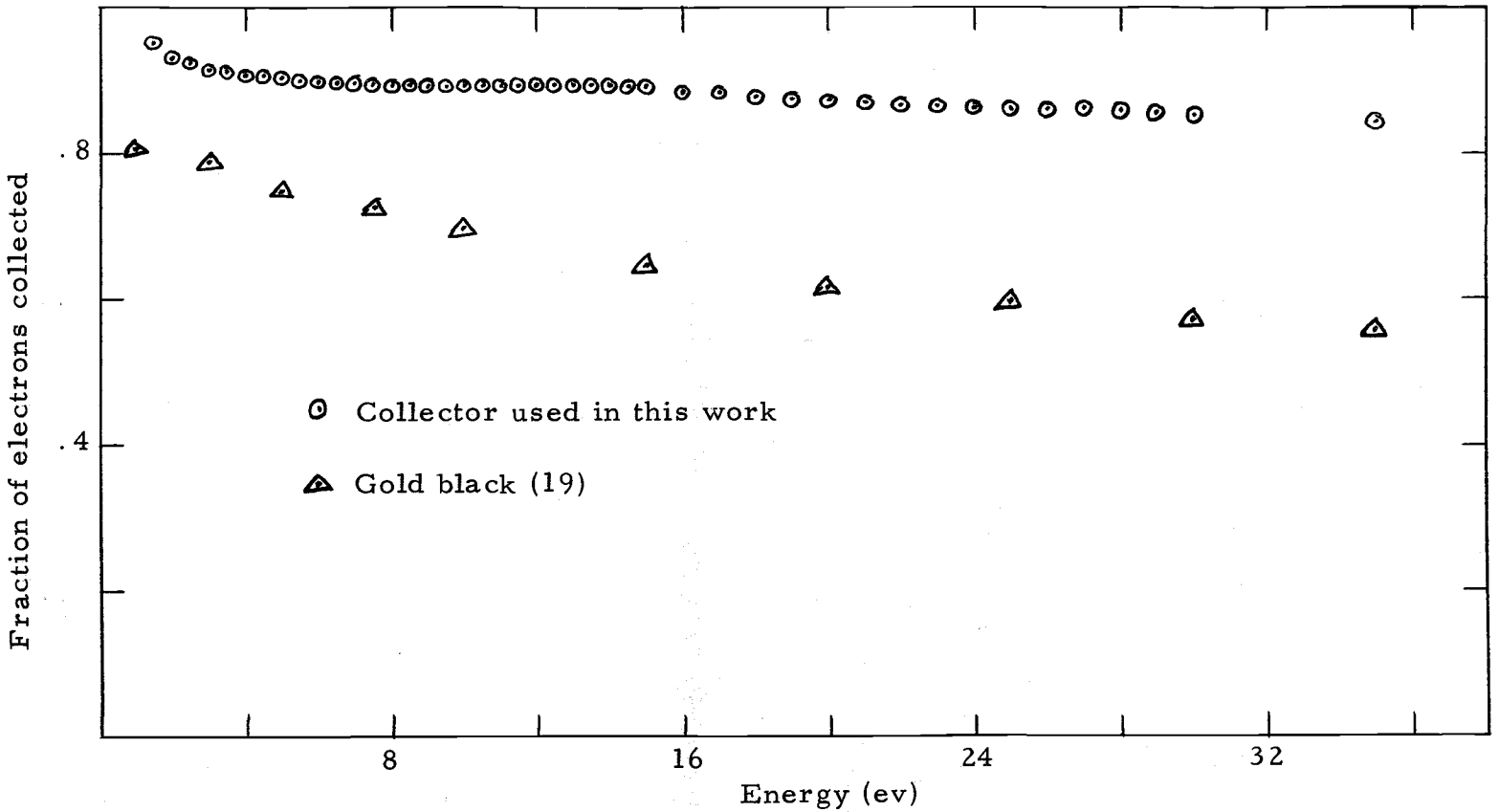

Figure 6. Electron collection efficiencies.

collector had the same area, and I_r/I_c was found always to be .01 or less (with the gun at the center of the guard sphere), the fraction of I_r which resulted from primary electrons had little influence on the total secondary emission coefficient δ. δ is defined as the fraction of electrons not collected by the collector and, therefore, from the above expression for the fraction collected, δ is given by $1 - I_c/(I_c+I_r+I_g)$. This expression, from the above arguments, yields a very close upperbound to the total secondary emission coefficient.

The Discharge Cell

A 7 cm diameter, 200 cc pyrex boiling flask, roughly spherical, was used to build the cell. First, a 12/5 ground glass ball joint was attached by a short glass tube blown into the flask. This ball joint served as the connection to the gas handling system and also supported the cell. The ground joint was not greased, to maintain gas purity, and was found not to leak. The flask was then cut in half so that the cathode assembly and guard ring could be installed; also, the neck of the flask was cut off to form the light port. A 3/4 inch aperture was cut through the top of the flask for installation of the anode and a 1/16 inch collar was ground to support it. A 1/4 inch kovar-to-pyrex seal and two platinium wires were blown into the flask to support the cathode assembly and to make electrical connections to the

heater and guard ring. The cathode assembly was welded to the kovar seal and consisted of, first, a stainless steel holder in which the heater, a ceramic disk wrapped with .015 inch tantalum wire, was mounted. On the top of the holder was mounted a 1-1/2 inch diameter stainless steel disk on which a 3/4 inch nickel disk was spot welded. See Figure 3. The nickel disk, which formed the cathode of the Townsend discharge, was treated with a mixture of Ba and Sr carbonate in a butyl acetate suspension to produce a low work function surface. The suspension was put on an area of about 3/8 inch diameter at the center of the nickel disk to act as the photoelectron emitting part of the cathode. The surface was activated by first being heated under vacuum to drive off the binder and to convert the carbonates to oxides and then by running a glow discharge for several hours at about 400 volts at 5×10^{-3} amps with about one torr of argon in the cell. The glow discharge was run only between the cathode and guard ring with a 3×10^{5} ohm current-limiting resistor so that the anode would not be damaged. This activated cathode, when illuminated by the 100 watt type SH Hanovia high pressure mercury vapor lamp, gave ample discharge current even at low E/N. The guard ring was a .02 inch thick stainless steel disk 1-1/2 inch OD with a 3/8 inch diameter aperture in its center, and was mounted 1/2 cm from the anode. Since the anode cathode spacing was 2 cm, the guard ring was held at 3/4 of the anode potential by a voltage divider. After the anode was

mounted, the guard ring and the back of the anode were platinum blacked to reduce electron reflection in the discharge. Torr Seal low vapor pressure resin was used to glue the cell together and to mount the guard ring and anode. After the cell was assembled, the electrical leads were run through aluminum tubes which ran from the bottom of the cell to feed-throughs in the vacuum chamber wall. To electrically isolate the leads from the tubes, the wires were tightly stretched and then glued with Torr Seal resin at both ends of the tubes. The cell was painted with GC Electronics silver conductive paint so that the entire cell was electrostatically shielded and at anode potential. Thus, no stray fields from the guard ring, cathode, or leads were able to appear in the analyzing region.

The Anode

Although this is part of the discharge cell, its importance to the experiment is so great that it is desirable to give it its own section. The method used to construct the anode and the conditions under which it must operate in order that the experiment succeed will be discussed here. The anode construction was started with a disk of 5 mil thick copper foil, gold plated in this case to a thickness of .193 mil. The gold thickness was determined by weighing a square centimeter of the foil. The gold surface was prepared for etching with Kodak negative photoresist. See Appendix A for preparation details.

The pattern in the photoresist was a square array of 243 apertures confined to a 1/4 cm diameter circular area; each aperture was 13 microns in diameter and they were spaced 160 microns center-to-center. Once the photoresist was on, the copper was etched away from the back side of the pattern by nitric acid, leaving a thin gold foil in the center of the anode disk. Then this gold foil was etched with a drop of cold aqua regia placed over the pattern of holes formed by the photoresist. The etching was watched under a microscope until the desired pattern of apertures appeared through the gold. Finally, the photoresist was removed with a mixture of grinding grit and trichloroethylene. Since in the etching process all apertures did not etch properly, the resulting pattern in the gold consisted of about 200 apertures with most about 13 microns in diameter, with some smaller, but none larger.

The criteria which the anode must satisfy are as follows:

1. Electrons and gas atoms must flow out of the pattern only by effusion.
2. The probability that an electron will reflect from the foil and be collected at the collector must be small.
3. The gas flow must not disturb the equilibrium of the discharge.
4. The electric field penetration of the apertures must be negligible.

The following arguments and tests show that the above conditions are met by the anode used. First, the usual criterion for effusive flow is that the aperture diameter be small compared to the mean free paths involved. From the cross section data of Graham and Ruhlig (8) for electrons in argon, the minimum free path is 300 microns at one torr pressure. Since the largest aperture size in the pattern is about 13 microns, the effusive flow criterion for a single aperture is certainly satisfied. However, a pattern of apertures was used, and since the criterion for effusive flow in this case is not clear, some experimental evidence was needed to determine whether each aperture acted independently. The ratio of collector current to anode current was calculated from the geometry and compared to experimental results. If each aperture acts independently, then the flux through the pattern is just proportional to the total area of the apertures and, thus:

$$I_e = \frac{\text{area of apertures}}{\text{area of anode}} I_a ,$$

where I_e is the effusive current and I_a is the anode current. As shown earlier, the collector current is proportional to $\sin^2\theta_m$ and, thus $I_c = \sin^2\theta_m I_e$. Taking 200 apertures of diameter 13 microns and the effective diameter of the anode to be 3/8 inch, we have $I_c/I_a = 7.4 \times 10^{-5}$. Since not all the apertures are this large, and the effective diameter of the anode is taken to be only as large as the

aperture in the guard ring, this calculated ratio should be an upper limit. Experimentally, the typical discharge current was 10^{-9} amps and the typical collector current (no retarding voltage) was 5×10^{-14} amps. These give a ratio of 5×10^{-5}, which varied little for different E/N's or pressures and compares favorably with the predicted ratio.

In order to perform the following calculations, the discharge cell's running temperature must be known. To determine this, a thermometer was placed in a mock-up cell and, after running for a day as if in an actual data run, the temperature of 0°C was read on the thermometer through the window in the vacuum chamber.

For the argon atoms, the total gas flow rate out of the pattern is calculated assuming effusive flow and is then compared with the flow rate determined by the manufacturer's calibration supplied with the Vacoa valve. Assuming a Maxwellian distribution of velocities for the argon atoms, the effusive flow rate R is $R = pA/\sqrt{2\pi m/kT}$ atoms/sec, where p is the gas pressure, A is the open area of the pattern of apertures, m is the mass of an argon atom, k is Boltzmann's constant, and T is the absolute gas temperature. Taking p to be 1 torr, T to be 273°K, and the area as before, $R = .885 \times 10^{17}$ atoms/sec or 3.29×10^{-3} cc/sec at STP. The Vacoa valve setting with about 3 lbs/sq inch gauge pressure on the inlet side and with 1 torr pressure on the outlet or cell side was measured.

From the typical leak rate chart supplied with the Vacoa valve, the leak rate at the measured setting should lie between $.82 \times 10^{-3}$ cc/sec at STP and 7.6×10^{-3} cc/sec at STP, the average being 3.4×10^{-3} cc/sec at STP, which compares well with that calculated above assuming effusive flow.

To investigate the second criterion we note that relatively few electrons collide with the sides of the apertures because the gold foil is very thin, the ratio of aperture diameter to foil thickness being 2.5:1. However, since the apertures were etched, the foil thickness at the sides of the apertures is thinner than elsewhere making the above ratio somewhat larger. Thus, with this ratio and the small probability of reflection from the platinium blacked anode, the chance of an electron bouncing off the foil and being collected by the collector is small and is neglected in this work.

To determine the effect of the gas flow on the equilibrium of the gas, the gas drift velocity is compared to the average molecular speed. To obtain an upper limit to the drift velocity, the gas is assumed to flow uniformly in a pipe of diameter equal to that of the aperture pattern. The total flow rate of 3.29×10^{-3} cc/sec at STP, from above, is adjusted to the typical discharge operating conditions of 1 torr pressure and 0°C temperature. With this flow rate of 2.5 cc/sec at 1 torr and 0°C, the flow velocity of the gas in the pipe is 42 cm/sec. Since the gas really does not travel in a pipe, the pipe

flow velocity is an upper limit to the gas drift velocity in the discharge cell. With a Maxwellian distribution of velocities for the argon atoms, the average molecular speed at 0°C is 3.8×10^4 cm/sec. Thus, the gas drift velocity is very small compared to the average molecular speed; therefore, the equilibrium of the argon gas is essentially undisturbed.

Finally, electric field penetration of the apertures was also considered. A scale model of an aperture was set up in an electrolytic tank. It was found that a uniform electric field had diminished to .67% of its value after penetrating 5 aperture diameters. Since 5 aperture diameters is about 1/5 of the minimum mean free path for electrons in argon, field penetration was judged insufficient to disturb the equilibrium of the discharge.

Electrical Circuits

The wiring diagram is shown in Figure 7. All wires were coaxial with the outer shielding grounded, and batteries were used for power sources because of their low noise levels. The discharge voltage was supplied by two 225 volt photoflash batteries wired in parallel. This voltage was controlled by a 1.5 megohm potentiometer. The discharge current was measured by a Keithly 600A electrometer and was held at about 10^{-9} amps by placing screens in front of the light source. The guard ring voltage was maintained by

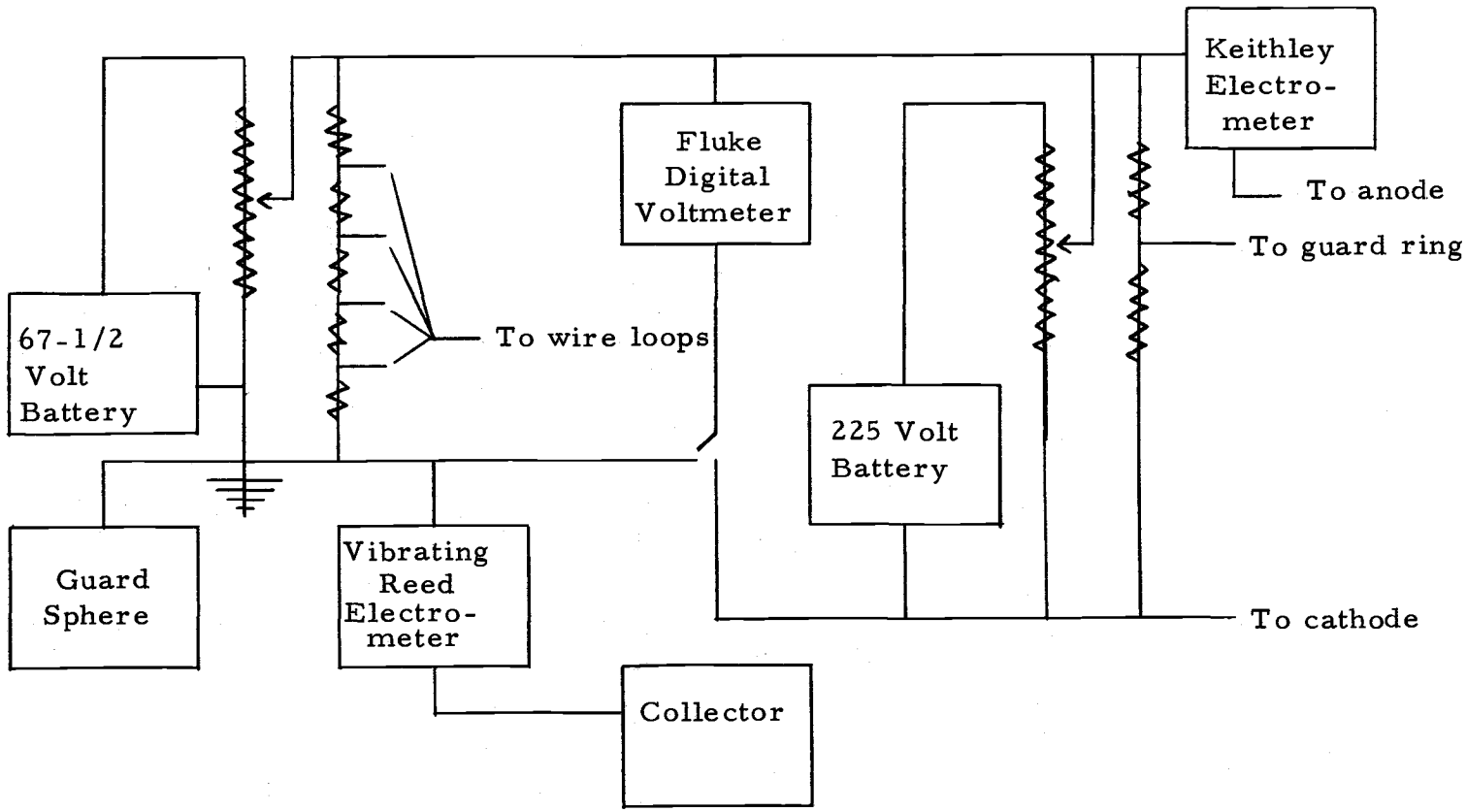

Figure 7. Block diagram of electrical circuits.

use of a voltage divider made from 1% resistors. The retarding voltage was supplied by a 67-1/2 volt battery controlled by a 10-turn, 10^5 ohm potentiometer. Twenty-two 1/8 watt 1% metal film resistors totaling about 1.8 megohms were used to form the voltage divider of the field shaping cone of wires. Both the retarding and discharge voltages were measured with a model 885AB Fluke DC differential voltmeter with an internal resistance of 10^7 ohms. The relative voltages were measured to .1% and the absolute voltages to 1%. The collector current was measured by a Cary model 31 vibrating reed electrometer connected by a 3 inch shielded lead directly to the collector. The background drift rate of the electrometer was less than 5×10^{-17} amps and the usual range of collector currents was from 10^{-15} amps to 5×10^{-14} amps. The collector and discharge currents were recorded continuously by a Leeds and Northrup speedomax G X_1-X_2 chart recorder.

DATA AND ANALYSIS

In this chapter, the following topics are discussed: the raw data, why these data indicate that the analysis in Chapter two was incomplete, the probable cause of the discrepancy, and the necessary modification of the analysis.

Before any data were taken the discharge was started and maintained for at least two hours to allow the light source, the discharge, and any charging insulators to come to equilibrium. The vibrating reed electrometer was used to measure the collector current directly by monitoring the voltage drop across a 10^{12} ohm Victoreen resistor. Whenever the retarding voltage was changed, a spurious collector current would appear due to the capacitive coupling of the cell and the collector; this current would die away within a few minutes after the retarding voltage was stabilized. The value of the collector current at each retarding voltage was taken from the chart only after it had remained constant for several minutes. See Figure 8. Each current was measured by alternating between succeeding pairs of retarding voltages two times, giving five current readings at each retarding voltage, three readings as the retarding voltage was increased and two as it was decreased. These five readings were then averaged and the average value was recorded as the current for that retarding voltage. If the five readings varied appreciably, then more time was

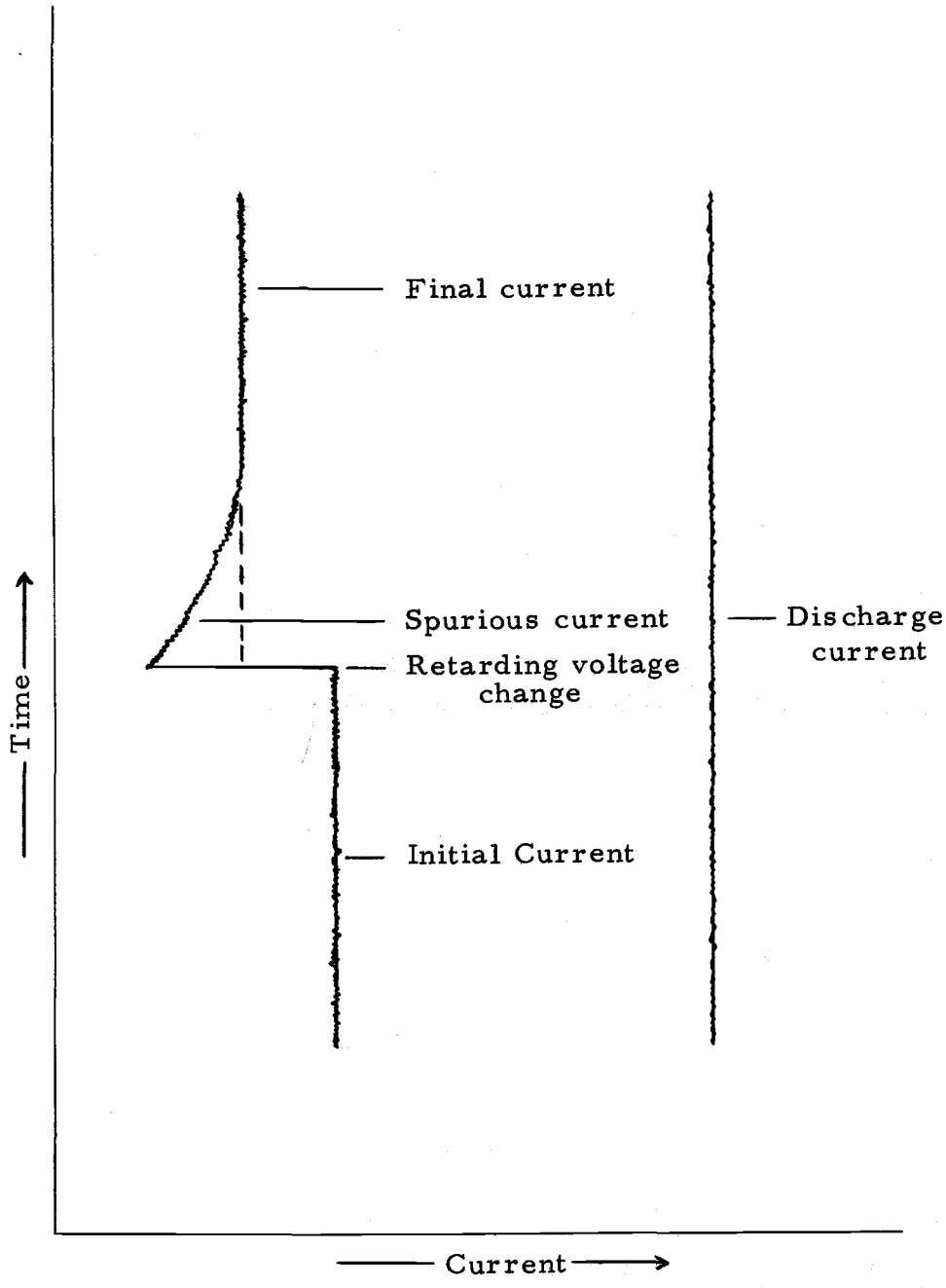

Figure 8. Typical chart recorder signal.

allowed for better equilibrium conditions to obtain. The typical variability when data were judged to be useful was 1% or less. The readings were taken at 1 volt intervals and were normalized to constant discharge current; however, for most runs the discharge current was stable enough that no adjustment was required. From Chapter two, the energy distribution function, to first approximation, is proportional to the derivative of the collector current times the reciprical of the square root of the energy; thus, if the distribution function is to remain finite at zero energy, the derivative must be zero at zero retarding field. Therefore, the collector current must saturate at zero retarding voltage; however, it was found that while the current started to saturate as the retarding potential was made to approach zero, see Figure 9, saturation did not occur until about 20 volts acceleration potential had been reached. Since the derivative was not zero at zero retarding field, it was clear that the theory did not accurately fit the experimental data, and some modification would be necessary. The theory assumed a perfect energy analyzer. In practice, simple retarding field energy analyzers always act as a diverging lens because electron paths are not always normal to equipotential surfaces. In the present case the equipotential surfaces are nearly plane parallel near the anode and become spherical near the collector. The cone of wires and the guard sphere tend to make the equipotential surfaces spherical and this causes the retarding field to

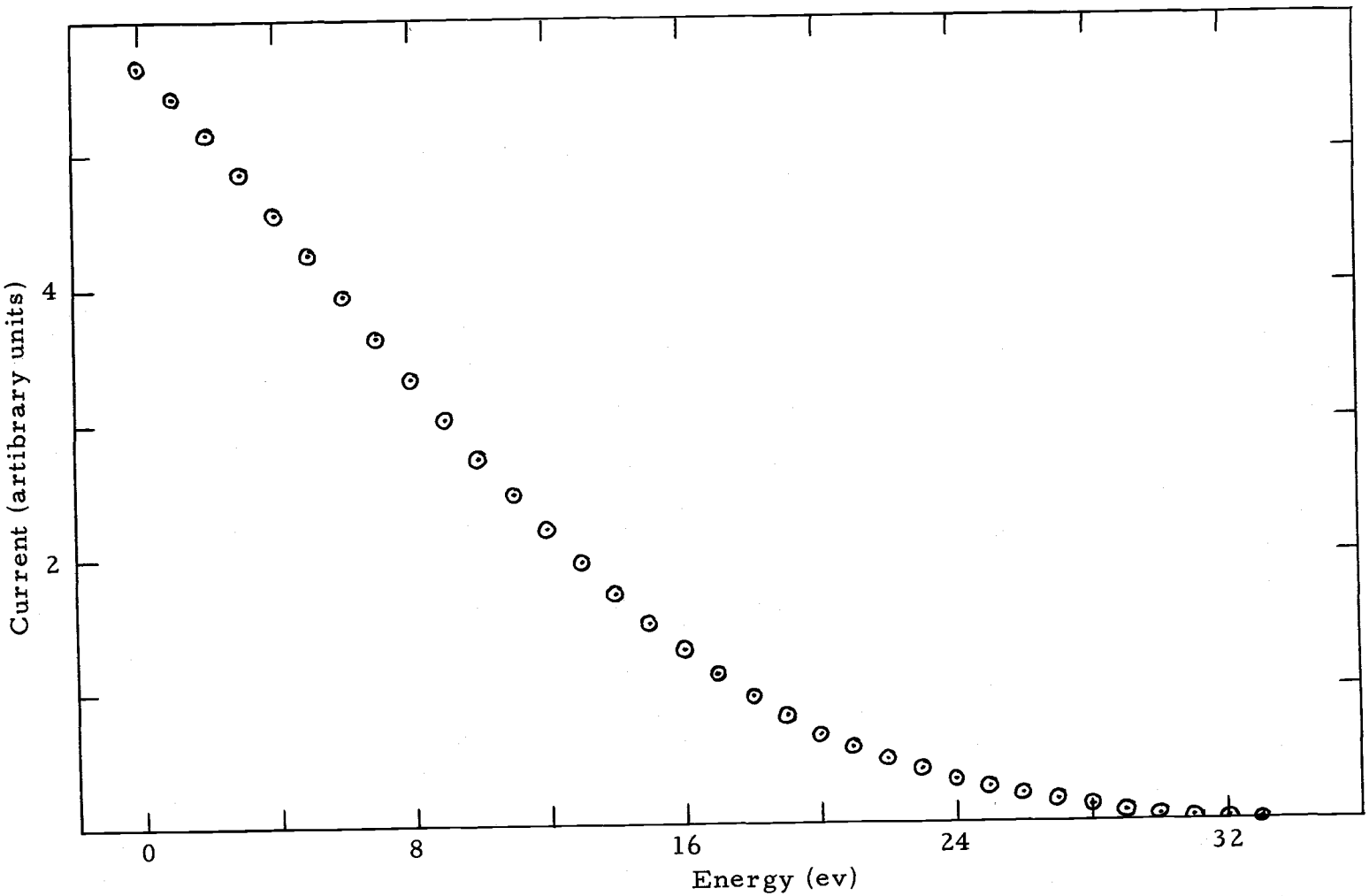

Figure 9. Typical collector current vs retarding voltage curve at E/N = 350 Td.

be strongest near the anode where the field is also least spherical. This field distortion gives rise to the divergence of the electron beam and, hence, the collector current can not saturate at zero retarding field. Analysis of the data with a non-ideal analyzer requires knowlegde of the fraction of electrons (at each energy and retarding field) not deflected away from the collector by the diverging lens effect. This fraction is called here the distortion function and is denoted $D(V,\epsilon)$, in which V is the retarding field voltage and ϵ is the electron energy. Thus, if the electron reflection from the collector is also included, the expression for the collector current becomes:

$$I(V) = \int_V^\infty \left[f_0(\epsilon) - \frac{.945(E/p)}{P_d(\epsilon)+Q_{in}(\epsilon)} \frac{df_0(\epsilon)}{d\epsilon} \right] \epsilon D(V,\epsilon) R(\epsilon - V) d\epsilon ,$$

where $R(\epsilon - V)$ is the collector efficiency and, since the reflectivity of the collector depends only on the energy at the collector, it is a function of $(\epsilon - V)$ only.

The determination of $D(V,\epsilon)$ involves taking retarding field measurements with no gas in the cell and then relating these to measurements made while gas is present. The two circumstances will here be called the no-gas case (ng) and gase case (g), respectively. For the no-gas case, for each electron energy, adjusted by varying the anode-cathode voltage, the collector current was measured and plotted as a function of retarding voltage. The distortion function is

then the current at retarding voltage V divided by the current at zero retarding voltage. For an ideal collector, for which there would be constant current for all V less than ϵ, the quotient would be unity. It was found experimentally that the distortion function was linear with respect to the retarding voltage up to about 1/2 volt from the electron energy, at which point the current dropped rapidly to zero. The value of the distortion function when the retarding voltage was equal to the electron energy could not be determined directly due to the narrow spread of electron energies; however, it was determined easily by extrapolating the linear curve. See Figure 10. This distortion function determined by the no-gas data cannot be directly applied to the gas case due to the difference in distribution of the electron flux in the two cases. The angular distribution is important, because the electrons normally collected near the edge of the collector are those most likely to be deflected and not collected, while those near the center can be deflected and still be collected. To relate the two cases, the approximate angular distributions of both cases and the approximate shape of the retarding field must be known. The flux in the gas case was assumed isotropic in Chapter one; however, a measurement of collector currents with a 4 inch and a 2 inch collector was made for both the no-gas and gas cases. In the gas case, the current to the 4 inch collector was about 4 times that to the 2 inch collector, which is expected for a nearly isotropic distribution. However, this is

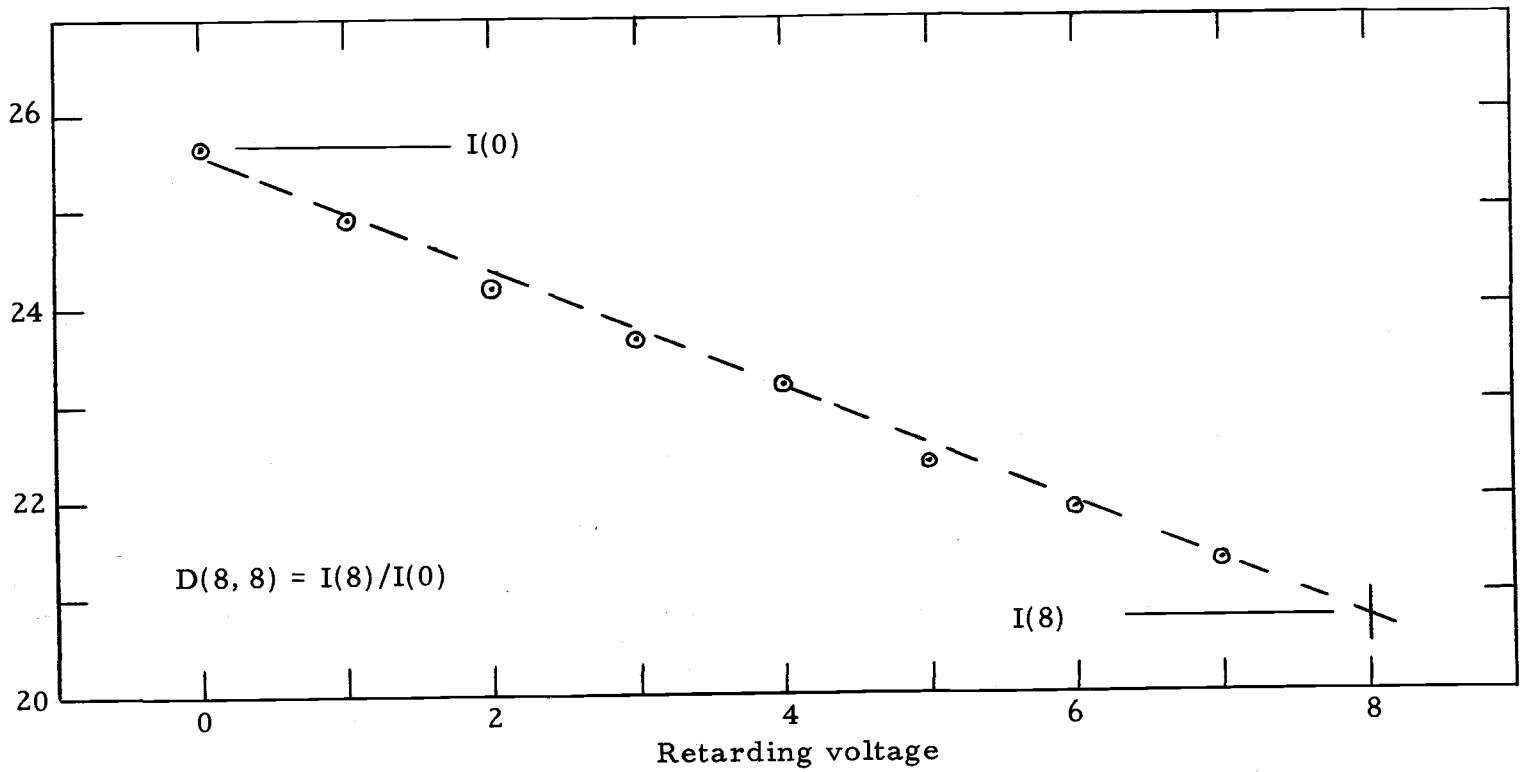

Figure 10. Sample curve for the determination of the no-gas distortion function for 8 volt electrons.

by no means a check on the expansion of the velocity distribution function, since this test is not very sensitive to the functional form of the angular distribution. In the no-gas case the 4 inch collector current was only about twice that of the 2 inch collector, indicating a forward peaked distribution. To determine the approximate form in the no-gas case, the ratio of currents was calculated using a distribution of the form $(\cos\theta)^n$, as follows:

$$\frac{I(4)}{I(2)} = \frac{\int_0^{\theta_4} (\cos\theta)^n \sin\theta d\theta}{\int_0^{\theta_2} (\cos\theta)^n \sin\theta d\theta} .$$

The parameter n was then adjusted until the ratio was equal to two, from which, n was found to be about eight. Approximate distortion functions may then be found by the following procedure. We assume that the retarding field just above the anode may be treated as a uniform field of height $h \ll R$, and with strength of the order of V/R, where R is the radius of the guard sphere. Next, we neglect the retarding effect of this region while we compute the deflection of an electron which enters the uniform field region at an angle θ to the field lines. The force component perpendicular to the undeflected trajectory of the electron is then $e(V/R)\sin\theta$, and this force acts for a time interval of $h/\sqrt{2\epsilon/m}$, producing a deflection of length

$\Delta = \frac{1}{2}(e/m)(V/R)\sin\theta(mh^2/2\epsilon) = \frac{1}{4}(h^2/R)(V/\epsilon)\sin\theta$, when ϵ is expressed in electron volts. Finally, the angle of deflection, θ_d, is

$$\theta_d = \Delta/(h/\cos\theta) = \frac{1}{4}(h/R)(V/\epsilon)\sin\theta\cos\theta \doteq \frac{1}{4}(h/R)(V/\epsilon)\theta$$

$$= k(V/\epsilon)\theta.$$

All electrons with $\theta + \theta_d \leq \theta_m$ are collected; these are all with $\theta \leq \theta_e$, where $\theta_e = \theta_m/(1+kV/\epsilon)$.

The distortion function has the form:

$$D(V,\epsilon) = \frac{\int_0^{\theta_e} f(\theta)\sin\theta d\theta}{\int_0^{\theta_m} f(\theta)\sin\theta d\theta},$$

where $f(\theta)$ is the angular distribution of the electron flux. The approximations made place an upper limit on θ_e and, thus this expression for $D(V,\epsilon)$ is an upper limit. For the gas case $f(\theta) = 1$ and thus:

$$D_g(V,\epsilon) = \frac{\int_0^{\theta_e} \sin\theta d\theta}{\int_0^{\theta_m} \sin\theta d\theta},$$

while for the no-gas case:

$$D_{ng}(V,\epsilon) = \frac{\int_0^{\theta_e} (\cos\theta)^8 \sin\theta d\theta}{\int_0^{\theta_m} (\cos\theta)^8 \sin\theta d\theta}$$

Since $(V/\epsilon) \leq 1$, $k < 1$, and $\theta_m = .473$ rad, after the integrals are performed, the functions are expanded keeping terms in θ_m^2 and $(kV/\epsilon)^2$ only. For the no-gas case:

$$D_{ng}(V,\epsilon) = 1 - 1.23(kV/\epsilon) + 1.05(kV/\epsilon)^2,$$

and, for the gas case:

$$D_g(V,\epsilon) = 1 - 2(kV/\epsilon) + 3(kV/\epsilon)^2.$$

These functions show $D(V,V)$ to be a constant; however, the no-gas data show $D(V,V)$ varying by 20% over the range of retarding potentials from 2 to 35 volts. This discrepancy can be easily predicted by assuming a uniform transverse electric field of only about .1 volt/cm in the analyzer region. A possible source for such a field could be a charged insulator. To take into account this effect, k was chosen to have the following form:

$$k = .118 + .304 \exp(-.205\epsilon),$$

such that $D_{ng}(V,V)$ agreed with the experimentally determined

no-gas distortion function. This k was then used in $D_g(V,\epsilon)$ to give the gas case distortion function as follows:

$$D_g(V,\epsilon) = 1 - 2[.118+.304\exp(-.205\epsilon)](V/\epsilon) + 3[.118+.304\exp(-.205\epsilon)]^2(V/\epsilon)^2.$$

All functions in the expression for the collector current have now been accounted for; thus, we are left with an integral-differential equation to solve in order to obtain $f_0(\epsilon)$. For purposes of manipulation, we define:

$$L(\epsilon) = \frac{.945(E/p)}{P_d(\epsilon)+Q_{in}(\epsilon)}$$

The expression for the collector current becomes:

$$I(V) = \int_V^\infty [f_0(\epsilon) - L(\epsilon)\frac{df_0(\epsilon)}{d\epsilon}]\epsilon D_g(V,\epsilon)R(\epsilon-V)d\epsilon,$$

or:

$$I(V) = \int_V^\infty f_0(\epsilon)\epsilon D_g(V,\epsilon)R(\epsilon-V)d\epsilon - \int_V^\infty \epsilon L(\epsilon)D_g(V,\epsilon)R(\epsilon-V)\frac{df_0(\epsilon)}{d\epsilon}\,d\epsilon.$$

Integrating the second integral by parts gives:

$$[f_0(\epsilon)\epsilon L(\epsilon)D_g(V,\epsilon)R(\epsilon-V)]_V^\infty - \int_V^\infty f_0(\epsilon)\frac{d}{d\epsilon}[\epsilon L(\epsilon)D_g(V,\epsilon)R(\epsilon-V)]d\epsilon.$$

Since $f_0(\epsilon) \to 0$ very rapidly for large ϵ and $R(0) = 1$, we have:

$$I(V) = Vf_0(V)L(V)D_g(V, V)$$

$$+ \int_V^\infty f_0(\epsilon)\left[\epsilon D_g(V, \epsilon)R(\epsilon - V) + \frac{d}{d\epsilon}\left[L(\epsilon)D_g(V, \epsilon)R(\epsilon - V)\epsilon\right]\right]d\epsilon .$$

For convenience, we define:

$$\text{Grand}\,(V, \epsilon) = \epsilon D_g(V, \epsilon)R(\epsilon - V) + \frac{d}{d\epsilon}\left[\epsilon L(\epsilon)D_g(V, \epsilon)R(\epsilon - V)\right]$$

$$\text{Fact}(V) = \left[VL(V)D_g(V, V)\right]^{-1}.$$

Then, the integral equation for $f_0(V)$ becomes:

$$f_0(V) = \text{Fact}(V)\left[I(V) - \int_V^\infty f_0(\epsilon)\text{Grand}(V, \epsilon)d\epsilon\right] .$$

The following outlines the method used to solve the integral equation.

First, the trapezoidal rule was used to replace the integral by a sum as follows:

$$f_0(V) = \text{Fact}(V)\left[I(V) - \frac{1}{2}f_0(V)\text{Grand}(V, V) - \sum_{\epsilon=V+1}^{40} f_0(\epsilon)\text{Grand}(V, \epsilon)\right] ,$$

or:

$$f_0(V) = \frac{\mathrm{Fact}(V)\left[I(V) - \sum_{\epsilon=V+1}^{40} f_0(\epsilon)\mathrm{Grand}(V,\epsilon)\right]}{1+\frac{1}{2}\mathrm{Fact}(V)\mathrm{Grand}(V,V)}.$$

Forty is chosen for the upper limit in this case because, for all data runs, $I(V)$ was zero before 40 volts retarding potential had been reached. We now have a set of simultaneous algebraic equations for the $f_0(V)$'s, ($V = 1$ to 40 in one volt steps). These were solved using a computer to do the calculations. First, $f_0(40)$ was set equal to zero and V set equal to 39; then, $f_0(39)$ was calculated. Knowing $f_0(40)$ and $f_0(39)$, $f_0(38)$ was calculated. This procedure was continued until all the $f_0(V)$'s ($V = 1$ to 40) were calculated. It is shown in Appendix B that this procedure gives a unique distribution function. After $f_0(V)$ was calculated, $f_1(V)$ was obtained by use of the equation which related it and $f_0(V)$.

RESULTS

In this chapter the distribution functions obtained by using the procedure developed in the last chapter are shown on graphs and in tabular form. The curious structure and the general forms of the distribution functions are discussed and compared with those obtained by others. Having the distribution functions and taking cross section data from the literature, the pertinent transport quantities are calculated and compared with other work.

Townsend discharges in argon gas were investigated over a range from 70 Td to 407 Td in steps of 70 Td. After the preliminary work, at most three data runs were made at each E/N, and at 140 Td and 210 Td the pressure and voltage were changed between runs while E/N was held constant to see if there was any pressure dependence. At 140 Td the pressure was changed from 2 torr to 1.5 torr and at 210 Td it was changed from 1.33 torr to 1 torr; no effect on the data was observed in either case. The data indicated some structure in the shapes of the approximate distribution functions, but at some values of E/N the structure did not reproduce when runs were taken on different days; however, at least two data runs matched well, even when they were taken weeks apart. The resulting normalized distributions, shown in Figure 11 and Tables 1 and 2, are drawn from an analysis of the best data runs which gave consistent

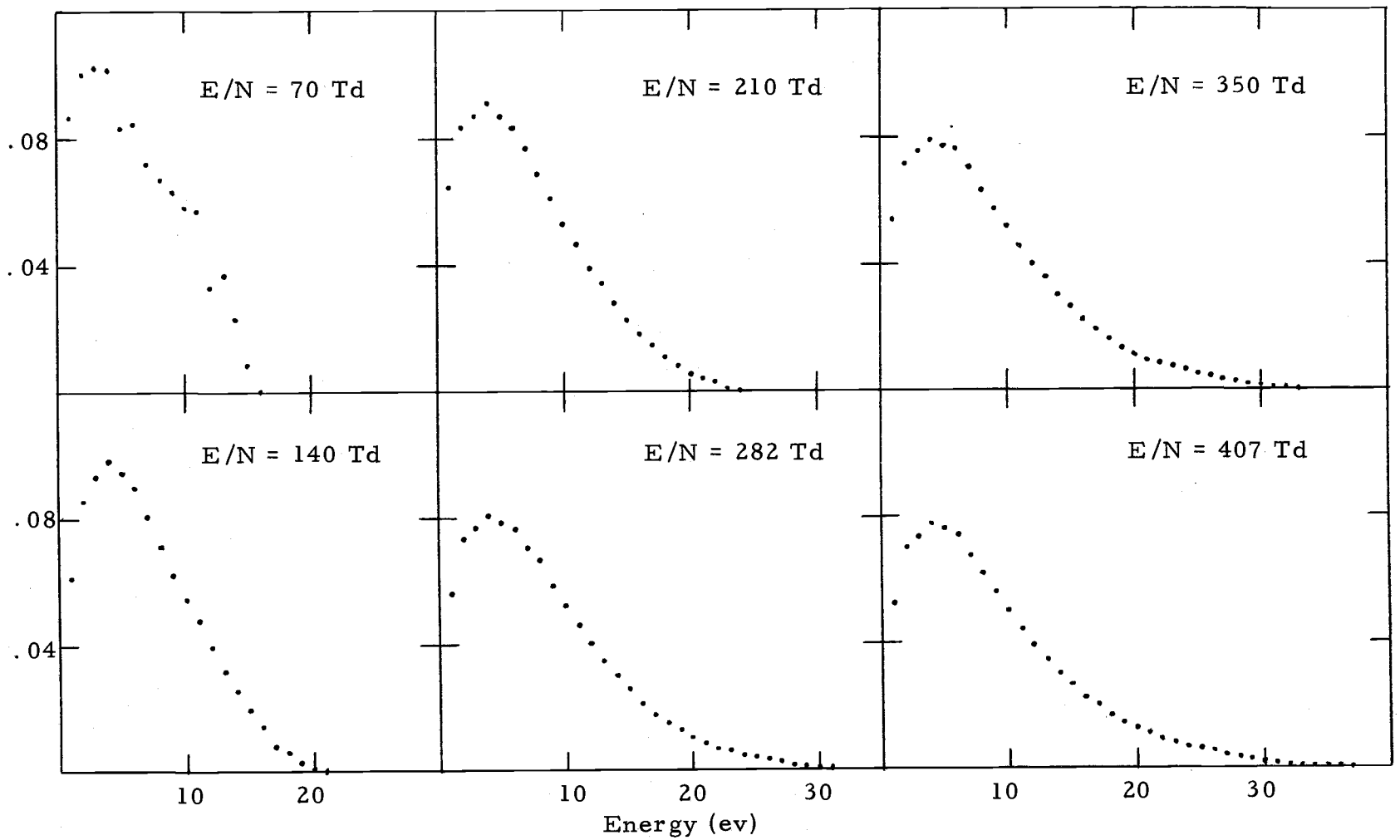

Figure 11. Normalized energy distribution functions using the GR diffusion cross section.

Table 1. Table of normalized electron distribution functions in argon using the GR diffusion cross section.

E/N	70 Td		140 Td		210 Td		282 Td		350 Td		407 Td	
ϵ	F_0	F_1	F_0	F_1	F_0	F_1	F_0	F_1	F_0	F_1	F_0	F_1
0	.0000	.0000	.0000	.0000	.0000	.0000	.0000	.0000	.0000	.0000	.0000	.0000
1	.0870	.0298	.0618	.0048	.0605	.0097	.0563	.0443	.0542	.0446	.0537	.0564
2	.1062	.0245	.0860	.0139	.0837	.0268	.0734	.0411	.0716	.0470	.0704	.0570
3	.1026	.0217	.0933	.0204	.0872	.0359	.0774	.0405	.0755	.0487	.0737	.0555
4	.1012	.0208	.0986	.0220	.0914	.0326	.0809	.0355	.0793	.0431	.0780	.0461
5	.0836	.0151	.0946	.0236	.0870	.0327	.0790	.0342	.0771	.0397	.0765	.0472
6	.0849	.0098	.0901	.0231	.0836	.0285	.0769	.0338	.0765	.0386	.0744	.0479
7	.0723	.0109	.0807	.0230	.0772	.0291	.0707	.0311	.0704	.0435	.0681	.0483
8	.0673	.0068	.0715	.0214	.0691	.0291	.0669	.0310	.0638	.0407	.0625	.0445
9	.0635	.0063	.0625	.0192	.0612	.0275	.0591	.0339	.0578	.0367	.0564	.0434
10	.0588	.0052	.0547	.0167	.0531	.0250	.0525	.0303	.0520	.0350	.0501	.0420
11	.0572	.0130	.0481	.0171	.0467	.0237	.0463	.0284	.0463	.0349	.0441	.0384
12	.0336	.0112	.0397	.0180	.0395	.0217	.0407	.0271	.0405	.0321	.0392	.0341
13	.0374	.0062	.0323	.0162	.0347	.0206	.0353	.0260	.0361	.0318	.0349	.0342
14	.0234	.0161	.0262	.0151	.0284	.0221	.0306	.0242	.0306	.0308	.0302	.0312
15	.0088	.0137	.0200	.0146	.0229	.0200	.0261	.0235	.0268	.0281	.0271	.0299
16	.0000	.0054	.0147	.0138	.0182	.0162	.0219	.0212	.0224	.0265	.0229	.0288
17		.0000	.0092	.0113	.0149	.0156	.0186	.0185	.0193	.0229	.0201	.0250
18			.0064	.0084	.0109	.0147	.0158	.0173	.0164	.0218	.0173	.0235
19			.0033	.0086	.0082	.0119	.0130	.0154	.0136	.0201	.0150	.0203
20			.0004	.0049	.0056	.0092	.0110	.0131	.0114	.0168	.0131	.0179
21			.0000	.0007	.0043	.0057	.0090	.0115	.0096	.0118	.0114	.0164
22				.0000	.0032	.0058	.0075	.0088	.0086	.0093	.0097	.0153
23					.0018	.0070	.0063	.0071	.0074	.0089	.0083	.0120

(Continued)

Table 1. Continued.

E/N	70 Td		140 Td		210 Td		282 Td		350 Td		407 Td	
ϵ	F_0	F_1	F_0	F_1	F_0	F_1	F_0	F_1	F_0	F_1	F_0	F_1
24					.0000	.0038	.0052	.0060	.0064	.0083	.0072	.0083
25						.0000	.0044	.0057	.0053	.0065	.0065	.0077
26							.0033	.0045	.0047	.0051	.0054	.0084
27							.0028	.0037	.0039	.0063	.0045	.0060
28							.0019	.0037	.0028	.0060	.0040	.0055
29							.0013	.0033	.0020	.0048	.0031	.0061
30							.0006	.0032	.0013	.0040	.0023	.0058
31							.0000	.0014	.0007	.0030	.0015	.0043
32								.0000	.0003	.0020	.0011	.0028
33									.0000	.0008	.0006	.0022
34										.0000	.0004	.0014
35											.0002	.0007
36											.0003	.0007
37											.0000	.0008
38												.0000

Table 2. Table of normalized electron distribution functions in argon using the MB diffusion cross section.

E/N	70 Td		140 Td		210 Td		282 Td		350 Td		407 Td	
ϵ	F_0	F_1	F_0	F_1	F_0	F_1	F_0	F_1	F_0	F_1	F_0	F_1
0	.0000	.0000	.0000	.0000	.0000	.0000	.0000	.0000	.0000	.0000	.0000	.0000
1	.0748	.0455	.0538	.0146	.0501	.0208	.0445	.0507	.0422	.0501	.0412	.0598
2	.0929	.0252	.0739	.0069	.0688	.0154	.0593	.0233	.0568	.0240	.0553	.0291
3	.1016	.0211	.0893	.0165	.0810	.0278	.0705	.0299	.0677	.0341	.0658	.0374
4	.0974	.0215	.0912	.0220	.0823	.0310	.0718	.0325	.0693	.0381	.0678	.0401
5	.0831	.0139	.0906	.0205	.0814	.0269	.0729	.0268	.0704	.0295	.0695	.0345
6	.0828	.0088	.0848	.0188	.0773	.0215	.0703	.0246	.0694	.0266	.0674	.0327
7	.0717	.0085	.0790	.0159	.0748	.0185	.0678	.0178	.0673	.0258	.0653	.0277
8	.0673	.0048	.0714	.0144	.0687	.0184	.0664	.0185	.0629	.0242	.0619	.0258
9	.0636	.0043	.0631	.0115	.0622	.0158	.0599	.0189	.0586	.0191	.0577	.0229
10	.0581	.0008	.0568	.0083	.0557	.0127	.0553	.0152	.0550	.0167	.0534	.0211
11	.0669	.0073	.0520	.0080	.0506	.0116	.0500	.0133	.0505	.0164	.0482	.0184
12	.0308	.0063	.0442	.0087	.0437	.0096	.0456	.0123	.0455	.0141	.0442	.0151
13	.0439	.0004	.0367	.0071	.0403	.0085	.0403	.0115	.0420	.0141	.0404	.0155
14	.0316	.0074	.0316	.0067	.0343	.0106	.0361	.0111	.0364	.0146	.0356	.0145
15	.0141	.0078	.0246	.0065	.0276	.0095	.0309	.0109	.0322	.0130	.0323	.0137
16	.0000	.0036	.0198	.0065	.0230	.0067	.0269	.0095	.0277	.0121	.0279	.0131
17		.0000	.0125	.0054	.0200	.0071	.0230	.0083	.0241	.0105	.0250	.0116
18			.0101	.0036	.0148	.0071	.0200	.0079	.0209	.0103	.0214	.0110
19			.0061	.0051	.0117	.0061	.0165	.0075	.0174	.0104	.0189	.0097
20			.0009	.0034	.0078	.0048	.0140	.0064	.0140	.0090	.0162	.0086
21			.0000	.0005	.0063	.0024	.0114	.0061	.0115	.0059	.0143	.0084
22				.0000	.0052	.0028	.0091	.0047	.0104	.0046	.0117	.0088
23					.0033	.0047	.0077	.0037	.0088	.0046	.0096	.0067

(Continued)

Table 2. Continued.

E/N	70 Td		140 Td		210 Td		282 Td		350 Td		407 Td	
ϵ	F_0	F_1	F_0	F_1	F_0	F_1	F_0	F_1	F_0	F_1	F_0	F_1
24					.0000	.0030	.0063	.0031	.0076	.0046	.0082	.0042
25						.0000	.0054	.0032	.0061	.0036	.0075	.0041
26							.0039	.0027	.0056	.0025	.0062	.0050
27							.0035	.0021	.0046	.0037	.0050	.0034
28							.0024	.0023	.0034	.0039	.0046	.0031
29							.0018	.0022	.0024	.0031	.0035	.0039
30							.0008	.0024	.0016	.0027	.0027	.0039
31							.0000	.0011	.0009	.0022	.0016	.0030
32								.0000	.0004	.0015	.0012	.0019
33									.0000	.0007	.0007	.0016
34										.0000	.0005	.0010
35											.0002	.0005
36											.0003	.0005
37											.0000	.0007
38												.0000

shape. In order to analyze the data, the diffusion and total inelastic cross sections must be used. The total inelastic cross section as obtained from (6) was used consistently throughout this work; however, due to the large variance in the values reported for the diffusion cross section, the data analysis was performed using two choices of quite different diffusion cross sections as given by either Massey and Burhop (15) or Graham and Ruhlig (8). These are referred to as MB and GR, respectively, and were chosen because they seem to represent reasonable high and low estimates to the true cross section, respectively. The shape of the energy distribution function for a fixed value of E/N is not strongly dependent on the choice of diffusion cross section and varies by no more than 10% for the two diffusion cross sections used here. See Figure 12. In reproducing data runs it was noticed that the voltage scale increased by about one volt after several hours of running with gas in the cell, and it was postulated that the absorption of argon gas on the platinum black surface of the collector changed its work function and thus shifted the voltage scale. Due to this effect and the usual contact potentials, all absolute voltage scales are to be taken at nominal ± one volt. After horizontal shifting of the curves to account for the effect just described, most data points reproduced to within about one dot width on Figure 11, except at large ϵ where the uncertainty is greater due to the small residual current at large retarding field.

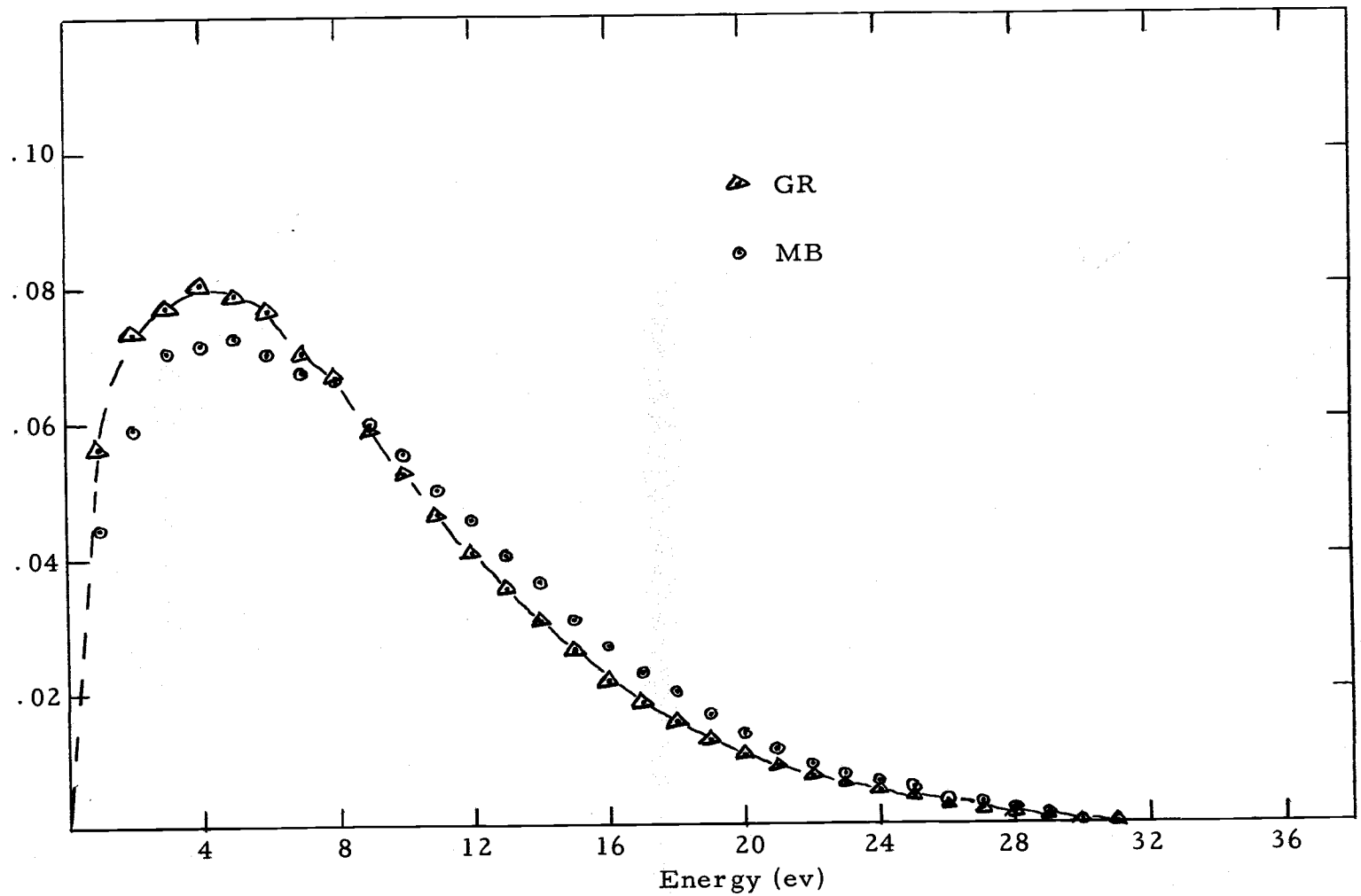

Figure 12. Normalized energy distribution functions at E/N = 282 Td for two choices of the diffusion cross section.

Structure in the form of the distribution functions was suggested by the analysis of the data using the first approximation procedure mentioned in Chapter two. This "first look" indicated sharp drops in the distribution functions at approximately 7, 12, and 15 volts with, perhaps, some above 15 volts. With the complete analysis of the data, most of the structure was observed in the anisotropic part $F_1(\epsilon)$, see Figure 13, with only a hint of structure in the energy distribution functions except at low E/N. All energy distribution functions show at least a slight "break" at about 7 volts, see Figure 11; however, the structure is more pronounced when the MB cross section is used. See Figure 12. While there is significant error in the determination of $F_1(\epsilon)$, the structure in $F_1(\epsilon)$, particularly at the voltages mentioned above, is substantiated by the abrupt changes observed in the derivative of the discharge current. The origin of this structure is unknown; however, the first excitation and ionization potentials in argon are at 11.5 and 15.7 volts, respectively, and the excitation potentials of water, oxygen, and nitrogen are around 7 volts. While there is no direct evidence, this occurrence of the structure at the approximate onset energies of the inelastic processes in argon and the most probable impurities suggests a connection. It seems reasonable that any structure in the distribution functions is likely to be due to inelastic collisions. The gross shapes of the energy distribution functions, although somewhat dependent on the choice of

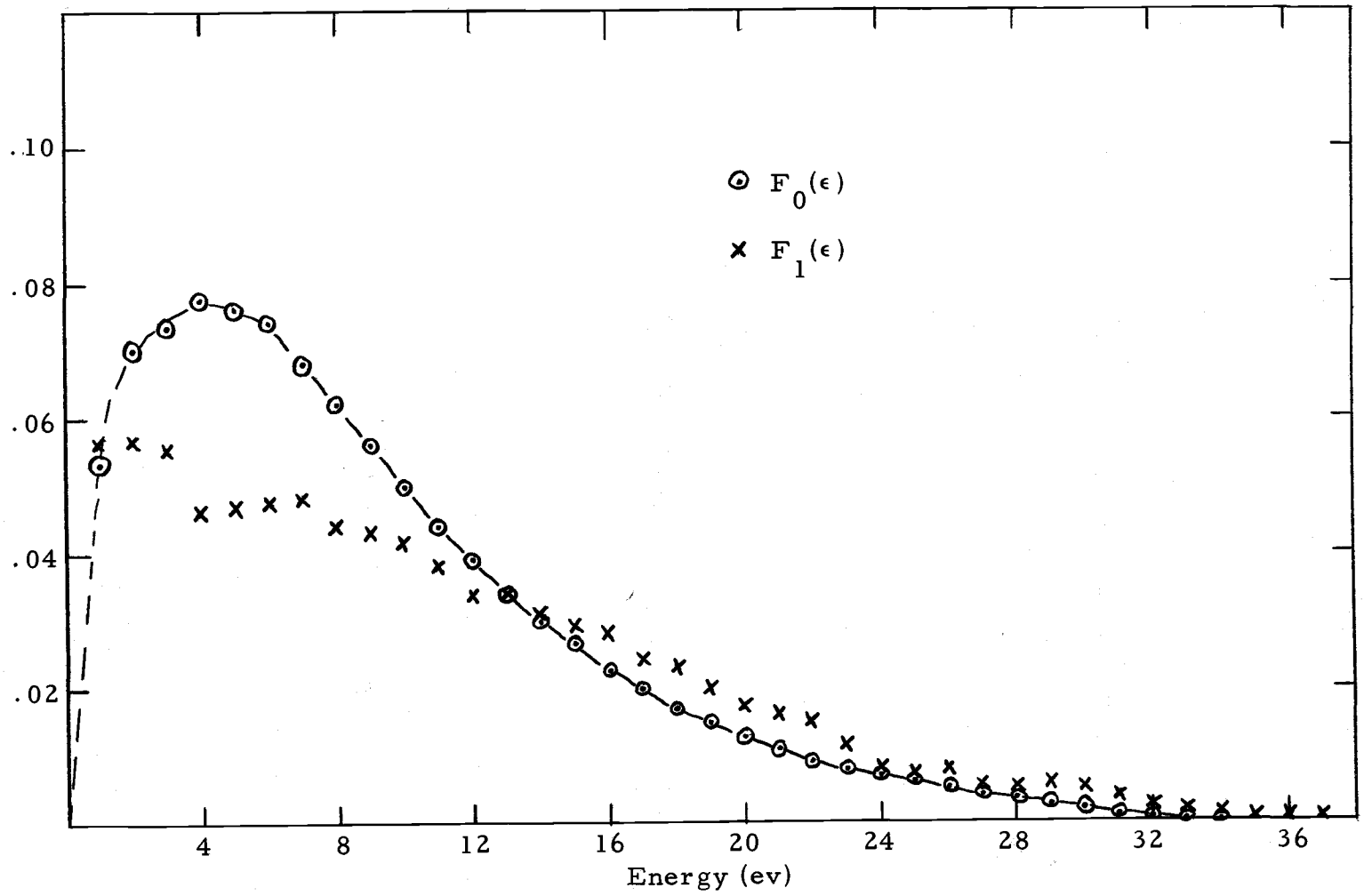

Figure 13. Normalized distribution functions $F_0(\epsilon)$ and $F_1(\epsilon)$ at E/N = 407 Td.

diffusion cross section, agree, except at low energies, where the distortion theory used in the analysis is of questionable validity, with those calculated by Golant (7), and by Fletcher and Burch (6); however, the very sharp cut-off found by Heylen and Lewis (9) in their calculated energy distribution functions was not observed.

The following transport quantities are calculated from the experimental distribution functions using both MB and GR diffusion cross sections: α/p_0, $p_0\mu$, p_0D, $\bar{\epsilon}$, and D/μ, where p_0 is the gas pressure in torr corrected to a temperature of 0°C, α is Townsend's first ionization coefficient, μ is the electron mobility, D is the electron diffusion constant, and $\bar{\epsilon}$ is the average electron energy. These quantities are computed (with the aid of a computer for determination of values of integrals) from the usual equations, as follows:

$$\mu p_0 = 1.98 \times 10^7 \int_0^\infty \frac{\epsilon}{P_d(\epsilon)} \frac{d}{d\epsilon}[f_0(\epsilon)]d\epsilon \quad \frac{cm^2\text{-torr}}{volt\text{-}sec},$$

$$p_0 D = 1.98 \times 10^7 \int_0^\infty \frac{\epsilon}{P_d(\epsilon)} f_0(\epsilon)d\epsilon \quad \frac{cm^2\text{-torr}}{sec},$$

$$\alpha/p_0 = \frac{5.94 \times 10^7}{(E/p)\mu} \int_0^\infty \epsilon Q_i(\epsilon) f_0(\epsilon)d\epsilon \quad \frac{1}{cm\text{-torr}},$$

where $P_d(\epsilon)$ is the diffusion cross section in units of cm^{-1}, $Q_i(\epsilon)$ is the ionization cross section in units of cm^{-1}, ϵ is in units of electron volts, and the integrated distribution functions have been normalized to unity as follows:

$$1 = \int_0^\infty F_0(\epsilon)d\epsilon .$$

These quantities are tabulated in Table 3, where they are expressed in the above units using the gas pressure and, also, in terms of the gas concentration. For the values of $N\mu$ and ND in this range of E/N there is no experimental results to compare; however, experimental results at E/N of 11 Td and below (2) indicate that the values found here are at least reasonable and in the correct range. The quotient D/μ is a measure of the average energy of the electrons, and the quotient of D/μ by $\bar{\epsilon}$ gives an average value of .700 with a maximum variance from this value of 5% over the range of E/N studied when the GR diffusion cross section is used. When the MB diffusion cross section is used, the average value for this quotient is .890 with a maximum variance from this value of 13%. For comparison only, D/μ by $\bar{\epsilon}$ for the Druyesteyn distribution is .736 and for the Maxwellian .667, although neither of these distributions is valid in this range of E/N. Of the transport quantities, the only one which has been experimentally determined in argon for our range of E/N is α/N. The values of α/N as determined by use of the GR diffusion cross section are small compared with the experimental curve obtained by Kruithof and Penning (11) and are large when the MB diffusion cross section is used. See Figure 14.

Table 3. Table of transport quantities.

E/N	$p\mu \times 10^{-5}$	$pD \times 10^{-6}$	α/p	D/μ	$N\mu \times 10^{-22}$	$ND \times 10^{-22}$	$\alpha/N \times 10^{17}$	$\bar{\epsilon}$	$(D/\mu)/\bar{\epsilon}$
The following were calculated using the GR diffusion cross section									
70 Td	4.23	1.83	0.00	4.32	1.50	6.46	0.00	6.17	.699
140 Td	3.85	1.93	.250	5.01	1.36	6.84	.706	6.83	.733
210 Td	3.97	2.08	.687	5.24	1.41	7.37	1.94	7.37	.711
282 Td	4.13	2.37	1.68	5.73	1.46	8.40	4.73	8.39	.684
350 Td	4.12	2.45	1.66	5.95	1.45	8.67	4.68	8.66	.687
407 Td	4.16	2.56	1.82	6.15	1.47	9.04	5.12	8.99	.685
The following were calculated using the MB diffusion cross section									
70 Td	3.12	1.77	0.00	5.65	1.105	6.25	0.00	6.52	.867
140 Td	2.29	1.69	.681	7.38	.810	5.99	1.92	7.29	1.012
210 Td	2.24	1.70	1.80	7.57	.794	6.00	5.07	8.03	.942
282 Td	2.22	1.72	3.89	7.76	.786	6.10	11.00	9.15	.848
350 Td	2.16	1.73	3.82	8.01	.766	6.13	10.80	9.47	.846
407 Td	2.17	1.76	4.10	8.10	.769	6.22	11.58	9.81	.825

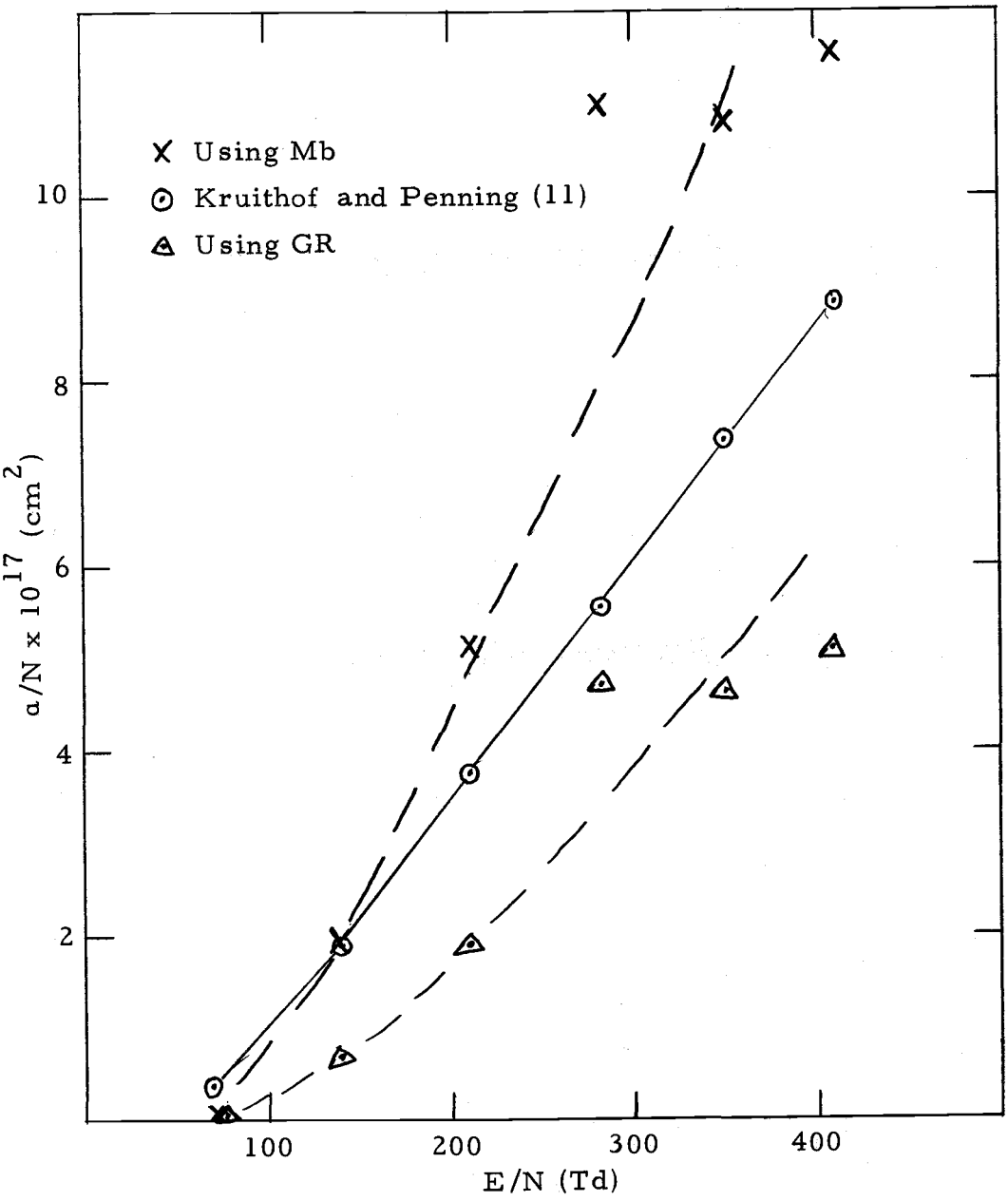

Figure 14. Townsend's first ionization coefficient vs E/N.

The values of α/N are particularly sensitive to the form of the high energy tails of the energy distribution functions and, therefore, are subject to large error; however, the above comparison indicates that the true diffusion cross section lies between these two cases as expected. Also, in this work a direct measurement of α/N was made at an E/N of 210 Td by holding E/N constant and varying E and p. The pressure was varied over a range from .4 torr to 1.33 torr in .1 torr steps. For a Townsend discharge at constant E/N and neglecting secondaries, the discharge current obeys the following equation $I = I_0 \exp(\alpha d)$, where I_0 is the electron current at the cathode and d is the anode-cathode spacing. Since α/p is a constant at constant E/p and constant temperature, a plot of discharge current on semi-log paper versus pressure should give a straight line with slope proportional to α/p. This type of plot is shown in Figure 15. The points plot as a straight line above about .8 torr, but are low at smaller pressures; this indicates that below .8 torr the electrons do not reach equilibrium with the gas in a distance which is negligible with respect to the anode-cathode spacing. The resulting effect is the same as if d in the expression for the current were made smaller. At .7 torr, d would have to be decreased by only 2% for the discharge current to be off the line by the amount indicated in Figure 15. Thus, in all data runs for determining the distribution functions, the electrons reached equilibrium

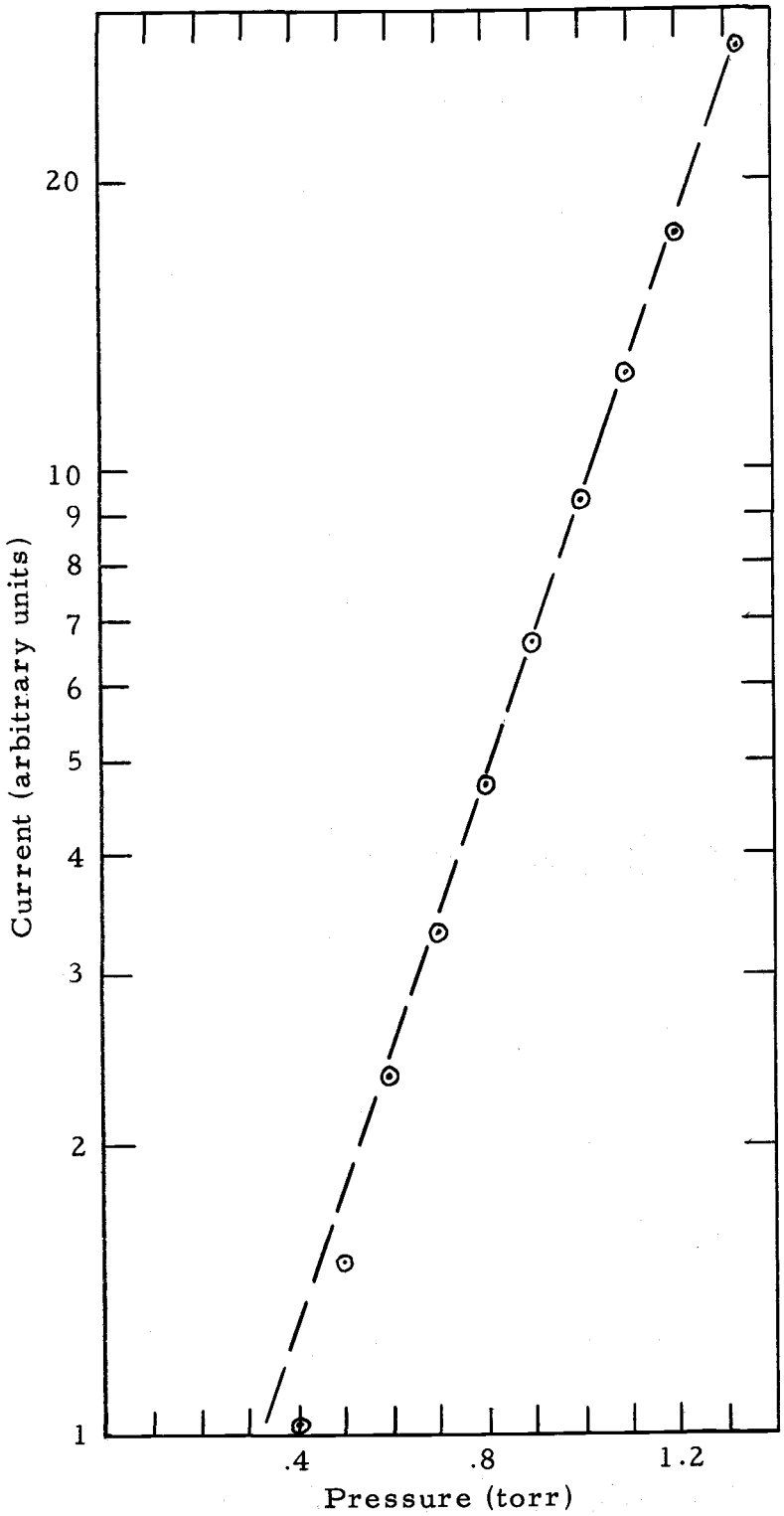

Figure 15. Semi-log graph of discharge current vs pressure at E/N = 210 Td.

well before arriving at the anode. The straight line of Figure 15 gave an α/N of 4.58×10^{-17} cm^{-1}, which lies between the calculated values using the two diffusion cross sections at E/N of 210 Td. This directly measured value of α/N need not be in exact agreement with that calculated from the distribution function because the impurity cross sections are not included; impurities might contribute greatly to any direct measurement of α/N while not significantly changing the form of the distribution function.

In addition to the data heretofore described, some runs were also taken at an E/N of 42 Td, and these showed pressure dependence and a double peaked distribution function. These data were not analyzed for inclusion in this work because the pressure dependence is not understood and because impurities become increasingly important at low E/N. It may be that the pressure dependence indicates that the electrons had not equilibrated with the electric field at this low E/N and pressure. For future work, a cell with a greater anode-cathode spacing might be used to investigate distribution functions at E/N's in this low range. Additionally, it is noted for future work that preliminary data indicated some additional structure when the argon gas was contaminated with carbon dioxide; investigations of molecular gases and gas mixtures might prove interesting in this connection. A general modification to the experiment would be to set up the cell and retarding region in a simpler geometric arrangement so

that the electric field in the retarding region is accurately known; some examples might be a parallel plate case and a concentric spheres case. In either case, the distortion theory as used earlier could be made exact, although possibly with some mathematical difficulty.

CONCLUSIONS

The work on the electron distribution functions in argon was concluded with the following results:

1. For electron energies from 0 to 60 electron-volts, the electron collection efficiency of platinum blacked stainless steel was shown to be much superior to that of gold black.
2. Electron energy distribution functions and the anisotropic drift terms of the velocity distribution functions were directly measured over their entire energy range, in argon, from E/N = 70 Td to 410 Td in 70 Td steps. The distribution functions were determined in the low energy range (0-8 electron-volts) by taking account of the diverging lens effect of the retarding field.
3. The shape of the experimentally determined energy distribution functions are generally in agreement with those calculated by Fletcher and Burch (6), and by Golant (7). The anisotropic part $F_1(\epsilon)$ was shown to be comparable to $F_0(\epsilon)$ in the range of E/N's investigated. Some unexplained structure appeared in the experimental distribution functions which seemed to be linked to the onset energies of the inelastic collision cross sections of argon and the most probable impurities. The structure was mainly confined to

the anisotropic part but was also evident to a smaller extent in the energy distribution functions. The very sharp cut-off at the first excitation level of argon predicted in the energy distribution functions calculated by Heylen and Lewis (9) was not observed.

4. The following transport quantities were determined for both Massey and Burhop's (15) and Graham and Ruhlig's (8) diffusion cross sections by using the corresponding experimental energy distribution functions along with the ionization cross section data of Rapp and Golden (18): α/N, $N\mu$, ND, and $\bar{\epsilon}$. Of these, only α/N has been experimentally determined in the range of E/N above about 40 Td in argon. The values of α/N obtained in the present investigation are either too large or too small, depending on the choice of diffusion cross section, compared with those determined by direct measurement by Kruithof and Penning (11). The indication is that the true cross section probably lies between the two choices.

BIBLIOGRAPHY

1. Abdelnabi and H.S.W. Massey. Inelastic Collisions of Electrons in Helium and Townsend's Ionization Coefficient. Proceedings of the Royal Society of London 66: 288-296. 1953. (Ser. A)

2. Brown, Sanborn C. Basic Data of Plasma Physics. New York, New York, Technology Press of the Massachusetts Institute of Technology and John Wiley and Sons, 1959. 336 p.

3. Cobine, James Dillon. Gaseous Conductors. New York, New York, Dover Publications, 1958. 606 p.

4. Engelhardt, A.G. and A.V. Phelps. Transport Coefficients and Cross Sections in Argon and Hydrogen-Argon Mixtures. The Physical Review 133: 375-380. Jan., 1964.

5. Engstrom, R.W. and W.S. Huxford. Time-Lag Analysis of the Townsend Discharge in Argon with Activated Caesium Electrodes. The Physical Review 58: 67-77. July, 1940.

6. Fletcher, John and D.S. Burch. Theoretical Electron Distribution Functions for Townsend Discharges in Argon. To be published.

7. Golant, V.E. Coefficient of Ionization and Mobility of Electrons in Argon. Soviet Physics Technical Physics 29: 680-682. Dec., 1959.

8. Graham, Walter J. and Arthur J. Ruhlig. Calculated Values of the Parameters of Noble Gas Discharges. The Physical Review 94: 25-29. April, 1954.

9. Heylen, A.E.D. and T.J. Lewis. Electron Energy Distributions and Transport Coefficients for the Rare Gases. Proceedings of the Royal Society of London 271: 531-550. 1963. (Ser. A)

10. Huxford, W.S. Townsend Ionization Coefficients in Cs-Ag-O Phototubes Filled with Argon. The Physical Review 55: 754-762. April, 1939.

11. Kruithof, A.A. and F.M. Penning. Determination of the Townsend Ionization Coefficient for Pure Argon. Physica 3: 515-533. June, 1936.

12. Loeb, Leonard B. Basic Processes of Gaseous Electronics. 2d. Berkeley, Calif., University of California Press, 1961. 1028 p.

13. Lonseth, A.T. Approximate Solutions of Fredholm-Type Integral Equations. Bulletin of The American Mathematical Society 60: 415-430. Sept., 1954.

14. Lummer, O. and F. Kurlbaum. Verhandlungen der Physikalische Gesellschaft 14: 66. 1895. (Cited in: Mellor, J.W. A Comprehensive Treatise on Inorganic and Theoretical Chemistry. Vol. 16. New York, Longmans, Green and Company, 1937. p. 49, 53)

15. Massey, H.S.W., E.H.S. Burhop and H.B. Gilbody. Electronic and Ionic Impact Phenomena. 2d. Vol. 1. Oxford, Clarendon Press, 1969. 664 p.

16. Milne, William E. Numerical Calculus. Princeton University Press, 1962. 393 p.

17. Nielsen, Russell A. Absolute Values of the Electron Drift Velocity in Nitrogen, Helium, Neon, and Argon. The Physical Review 50: 950-954. Nov., 1936.

18. Rapp, Donald and Paula Englander-Golden. Total Cross Sections for Ionization and Attachment in Gases by Electron Impact I Positive Ionization. The Journal of Chemical Physics 43: 1464-1479. Sept., 1965.

19. Roberts, T.D. and D.S. Burch. Total Secondary Emission Coefficient of Gold Black. The Review of Scientific Instruments 35: 1067. Aug., 1964.

20. Roberts, T.D. and D.S. Burch. Experimental Electron Energy Distributions for Townsend Discharges in Helium. The Physical Review 142: 100-104. Feb., 1966.

21. Simpson, J. Arol. Design of Retarding Field Energy Analysers. The Review of Scientific Instruments 32: 1283-1293. Dec., 1961.

22. Smit, J.A. Berechnung der Geschwindigkeitsverteilung der Elektronen bei Gasentladungen in Helium. Physica 3: 543-560. June, 1936.

23. von Engel, A. Handbuch der Physik. Vol. 21. Berlin, Springer-Verlag, 1956. 683 p.

24. Wannier, Gregory H. Statistical Physics. New York, John Wiley and Sons, 1966. 532 p.

25. Zollweg, R.J. Electron Reflection from Cesium Coated Polycrystallin Metals at Low Primary Energy. Journal of Applied Physics 34: 2590-2598. 1963.

APPENDICES

APPENDIX A

The negative photoresist process is as follows:

1. Make sure the surface is clean and free from finger prints, etc. Do not use aqueous solutions for cleaning; a suitable cleaning process is to scrub the surface with a cotton swab in a beaker of boiling trichloroethylene (TCE). The disk is stored in TCE until it is ready to be coated.
2. Immediately before coating, the disk is dried of TCE with a jet of air and then heated at 150°C for a few minutes.
3. The clean, dry disk is put on the spinner and covered with Kodak's KTFR negative photoresist which is diluted in the ratio 2 KTFR:1 Kodak's KMER thinner.
4. The spinner is set to approximately 7200 rpm and the disk is spun for 15 seconds.
5. The coated disk is then baked for ten minutes in a vacuum oven which is heated to between 50°C and 60°C.
6. The surface is exposed through a glass photographic plate which has the reduced pattern on it for 6 seconds by a high intensity lamp such as a sun lamp.
7. The surface is developed by sloshing the disk in a beaker of Kodak's KTFR developer for 1 minute and then rinsing in isopropyl alcohol.
8. Finally, the disk is baked for 4 minutes on a hotplate which is run at 150°C.

APPENDIX B

The following proof shows that the solution to the integral equation used to determine the distribution functions is unique.

Two solutions of the integral equation ($f(\epsilon)$ and $g(\epsilon)$) are assumed, such that $f(\epsilon) \neq g(\epsilon)$ for some ϵ. Thus:

$$f(V) = Fact(V)\left[I(V) - \int_V^\infty f(\epsilon)Grand(V, \epsilon)d\epsilon\right],$$

and

$$g(V) = Fact(V)\left[I(V) - \int_V^\infty g(\epsilon)Grand(V, \epsilon)d\epsilon\right].$$

Subtracting these two equations and setting $h(V) = f(V) - g(V)$ gives:

$$h(V) = -Fact(V)\int_V^\infty h(\epsilon)Grand(V, \epsilon)d\epsilon.$$

Using the trapezoidal rule to replace the integral and rearranging, gives:

$$h(V) = \frac{-\sum_{\epsilon=V+1}^{\infty} h(\epsilon)\frac{Grand(V, \epsilon)}{Grand(V, V)}}{\frac{1}{Fact(V)Grand(V, V)} + \frac{1}{2}}.$$

For $V \rightarrow \infty$:

$$\frac{1}{Fact(V)Grand(V, V)} \rightarrow 0,$$

$$\frac{\text{Grand}(V, \epsilon)}{\text{Grand}(V, V)} \rightarrow 1,$$

and, thus:

$$h(V) \rightarrow -2h(V),$$

which implies $h(V) \rightarrow 0$ for large V. Thus, if $h(V)$ is zero for some large V, then, by use of the equation for $h(V)$, $h(V-1)$ is zero. If $h(V-1)$ is zero, then $h(V-2)$ is zero. Hence, $h(V)$ is identically zero for all V. Therefore, $f(\epsilon) = g(\epsilon)$ For all ϵ and the solution is unique.